

# Ensemble-Based Annealed Importance Sampling\*

Haoxuan Chen<sup>†</sup> and Lexing Ying<sup>‡</sup>

**Abstract.** Sampling from a multimodal distribution is a fundamental and challenging problem in computational science and statistics. Among various approaches proposed for this task, one popular method is Annealed Importance Sampling (AIS). In this paper, we propose an ensemble-based version of AIS by combining it with population-based Monte Carlo methods to improve its efficiency. By keeping track of an ensemble instead of a single particle along some continuation path between the starting distribution and the target distribution, we take advantage of the interaction within the ensemble to encourage the exploration of undiscovered modes. Specifically, our main idea is to utilize either the snooker algorithm or the genetic algorithm used in Evolutionary Monte Carlo. We discuss how the proposed algorithm can be implemented and derive a partial differential equation governing the evolution of the ensemble under the continuous time and mean-field limit. We also test the efficiency of the proposed algorithm on various continuous and discrete distributions.

**Key words.** Annealed Importance Sampling, Markov Chain Monte Carlo, Evolutionary Monte Carlo, Ensemble-Based Monte Carlo, Mean-Field Limits

**MSC codes.** 65C05, 65C40, 65C60, 62P35

**1. Introduction.** Sampling from an unnormalized distribution numerically is a fundamental problem with applications in various fields, such as computational physics, Bayesian inference, uncertainty quantification, data assimilation, and machine learning. The most popular class of algorithms used for tackling this problem is the Markov Chain Monte Carlo (MCMC), whose thorough review can be found in [45, 51]. Common examples of MCMC methods include Unadjusted Langevin Algorithm (ULA) or Metropolis-Adjusted Langevin Algorithm (MALA) [78, 80, 81], Random-Walk Metropolis Algorithm [29, 79], Bouncy Particle Sampler [5], Hamiltonian or Hybrid Monte Carlo [2, 21, 71, 72, 82], Zig-Zag Sampler [4], etc. When the target distribution is (strongly) log-concave, it has been proved that most MCMC methods listed above can sample from the distribution efficiently [11, 13, 23, 24, 56, 58, 63, 98].

In contrast, when the target distribution is multimodal, the efficiency of standard MCMC methods is often limited by metastability, which refers to the demand of transiting between different high-probability modes separated by low-probability regions frequently. The main reason is that common MCMC methods are designed to sample a region based on its probability. Hence, they are able to explore a local high-probability mode efficiently, but they will only transit to another high-probability mode occasionally. To resolve metastability, numerous approaches have been proposed, such as mode-jumping (or mode-hopping) methods

---

\*Submitted to the editors.

**Funding:** The first author was partly supported by the T. S. Lo Graduate Fellowship Fund and the second author was partly supported by the National Science Foundation (NSF) under award number DMS-2011699 and DMS-2208163.

<sup>†</sup>Institute for Computational and Mathematical Engineering (ICME), Stanford University, Stanford, CA, 94305, USA ([haoxuanc@stanford.edu](mailto:haoxuanc@stanford.edu)).

<sup>‡</sup>Department of Mathematics and Institute for Computational and Mathematical Engineering (ICME), Stanford University, Stanford, CA, 94305, USA ([lexing@stanford.edu](mailto:lexing@stanford.edu), <https://web.stanford.edu/~lexing/>).

[3, 39, 76, 84, 85, 93, 94], cluster algorithms [88, 97], umbrella sampling methods [18, 66, 92], leap-point samplers [89, 90], transport map based methods [65, 73], machine learning based methods [1, 7, 26, 68, 95], to name a few.

Among various approaches proposed for sampling multimodal distributions, our main focus is on two classes of methods. The first class is the continuation (or tempering) method, whose main idea is to start with an easy-to-sample distribution and construct a continuous path between the initial distribution and the target distribution. Metropolis-Hastings (MH) Algorithm is then applied for continuation methods to move along the path. Compared to classical MCMC methods, continuation methods gradually transform the starting distribution into the target distribution when moving along the continuous path, which allows the samplers to explore the whole state space and transit between high-probability modes in the target distribution. One other advantage of continuation methods over traditional MCMC methods is that they are run over a finite time horizon instead of an infinite time horizon. Influential examples of continuation methods include Tempered Transitions [69], Simulated Tempering [31, 64, 69], Sequential Monte Carlo (SMC) [15, 20, 62], etc.

The second class is the ensemble-based (or population-based) methods, which keep track of multiple samplers instead of a single sampler throughout the sampling process. The invariant distributions associated with distinct samplers can be either the same or different as long as they are all related to the target distribution. Consequently, the ensemble-based methods utilize the interaction between different samplers as a way to speed up its convergence towards the target distribution. Examples of ensemble-based methods include (Sequential) Parallel Tempering [30, 38, 44], Conjugate Gradient Monte Carlo [50] and equi-energy sampler [42]. Some other ensemble-based methods proposed in recent studies include affine invariant and gradient-free sampling methods [9, 12, 22, 27, 28, 34, 41, 43, 55, 75], Stein Variational Gradient Descent and its variants [53, 54], etc. As the size of the ensemble approaches infinity, many studies [9, 10, 17, 27, 28, 49, 55, 57, 59, 60, 67, 75, 86, 96] have also investigated the mean-field limit of some ensemble-based sampling algorithms and obtained new insights.

This paper aims to improve the efficiency of Annealed Importance Sampling (AIS), which is one of the continuation methods and has been applied to many fields including computational physics [61, 99, 100, 101] and machine learning [8, 16, 19, 103]. As the standard AIS generates independent samples, it is natural to consider combining AIS with ensemble-based methods, which leverage the interaction between different samples, to improve the sampling efficiency. Similar to other continuation methods, standard AIS uses MH algorithms to sample from all the intermediate distributions along the continuation path connecting the initial distribution and the target distribution. Our main idea is to replace the MH algorithm used in AIS with a composition of standard MCMC algorithms and ensemble-based methods, which can exploit discovered modes locally, explore undiscovered modes globally, and balance the weights of the samplers in different modes. As a result, each intermediate distribution on the continuation path can be sampled in a more effective way, which leads to a more efficient AIS overall.

**1.1. Related Work.** The ensemble-based algorithm we proposed to replace the MH Algorithm used in AIS can be decomposed into three components: a local exploitation part, a global exploration part, and a part utilizing the birth-death process. The local exploitation part can be taken to be any standard MCMC algorithm, while our choice of the other two

parts is motivated by previous work.

The global exploration part, on the one hand, is used for eliminating the impact of metastability on sampling the intermediate distributions. Here, we select either the snooker algorithm [32] or the genetic algorithm [37] to be the global exploration part, which has been used in previous work [6, 91] to encourage exploration of missed modes and improve the efficiency of other sampling algorithms. In fact, both the snooker and the genetic algorithm are two important units of the Evolutionary Monte Carlo (EMC) method [46, 47], which belongs to the class of population-based Monte Carlo methods.

On the other hand, the part involving the birth-death process helps us move the particles within the discovered modes based on the weights of the modes. Our usage of the birth-death process here is inspired by previous literature blending the birth-death dynamics with sampling methods. For example, [59] proposed a hybrid algorithm by combining ULA with the birth-death dynamics, while [49] constructed an ensemble-based MCMC method that can be interpreted as a birth-death type dynamics under the mean-field limit. Among all the related studies, [8, 87] are the most relevant to our work. Specifically, [8, 87] proposed an improved version of AIS by incorporating it with a resampling strategy under the framework of SMC [15], which can also be treated as a way to balance the weights of the particles in the ensemble.

**1.2. Contributions.** Our main contributions in this paper are summarized below:

- We propose a novel sampling algorithm by combining Annealed Importance Sampling (AIS) with ensemble-based sampling methods. For the task of sampling continuous distributions, we prove that the empirical density formed by the ensemble converges to some target density and derive the partial differential equation (PDE) governing the evolution of the target density under the continuous time and mean-field limit.
- We provide numerical experiments to demonstrate that the new algorithm outperforms standard AIS on both continuous and discrete distributions with different dimensions.

**1.3. Organization of the paper.** This paper is organized as follows. In [section 2](#), we discuss a few existing sampling methods related to our work. In [section 3](#), we discuss the two ensemble-based AIS algorithms we developed and related theoretical properties under the continuous time and mean-field limit. In [section 4](#), we describe the numerical results to exhibit the practical performance of the new algorithms we proposed. Conclusions and discussions for future work can be found in [section 5](#).

**1.4. Preliminaries and Notations.** Below, we introduce a few preliminaries and list some basic notations used throughout this paper. Let  $p(\cdot) \propto e^{-U(\cdot)}$  be the target distribution we aim to sample from, where  $U : \mathcal{X} \rightarrow \mathbb{R}$  is the associated energy function and  $\mathcal{X}$  is the state space. Let  $d \in \mathbb{N}$  be some fixed integer. For continuous target distributions, we consider the case when  $\mathcal{X} = \mathbb{R}^d$ . For discrete target distributions, we consider the case when  $\mathcal{X} = \{-1, 1\}^d$ , i.e.,  $\mathcal{X}$  is binary-coded. For any domain  $\Omega \subset \mathbb{R}^d$ , the boundary of  $\Omega$  is denoted by  $\partial\Omega$ .

We use  $\langle \cdot, \cdot \rangle$  and  $\|\cdot\| = \sqrt{\langle \cdot, \cdot \rangle}$  to denote the standard dot product and the Euclidean norm in  $\mathbb{R}^d$ , respectively. The standard normal distribution in  $\mathbb{R}^d$  is represented by  $\mathcal{N}(\mathbf{0}, \mathbf{I}_d)$ , where  $\mathbf{I}_d$  is the identity matrix of size  $d \times d$ . For any  $a \in \mathbb{R}^d$ , we use  $\delta_a(\cdot)$  to denote the Dirac delta distribution at point  $a$ . For any function  $f : \mathbb{R}^d \rightarrow \mathbb{R}$ , the support of  $f$  is defined as  $\text{supp}(f)$ .

For any time-dependent path  $x = x(t) : [0, 1] \rightarrow \mathbb{R}^d$  in  $\mathbb{R}^d$ , we use  $\dot{x} = \frac{dx}{dt}$  to denote the time derivative of the path. For any time-dependent function  $g = g(x, t) : \mathbb{R}^d \times \mathbb{R} \rightarrow \mathbb{R}$ , we use  $\nabla_x g$ ,  $\nabla_x \cdot g$  and  $\Delta_x g$  to denote the spatial derivative, divergence and laplacian of  $g$ , i.e., the derivatives are taken with respect to the spatial variable  $x$ . The space of all the probability measures on  $\mathbb{R}^d$  is defined as  $\mathcal{P}(\mathbb{R}^d)$ . Furthermore, we use  $\mathcal{B}(\mathcal{P}(\mathbb{R}^d), \mathbb{R})$  to represent the space of all the functionals  $F : \mathcal{P}(\mathbb{R}^d) \rightarrow \mathbb{R}$ . For any  $N \in \mathbb{N}$ , the space of all the empirical probability measures that can be written as a weighted sum of  $N$  Dirac delta distributions is denoted by

$$\mathcal{P}_N(\mathbb{R}^d) := \left\{ \sum_{i=1}^N \gamma_i \delta_{a_i} : \sum_{i=1}^N \gamma_i = 1, \gamma_i > 0, a_i \in \mathbb{R}^d, \forall 1 \leq i \leq N \right\}.$$

**2. Review of Related Sampling Methods.** This section is devoted to investigating several examples of continuation and ensemble-based sampling methods that are most relevant to our work. In the first subsection, we describe Annealed Importance Sampling (AIS) [70]. In the second subsection, we provide a review of the snooker algorithm [32], and the genetic algorithm [37].

**2.1. Annealed Importance Sampling (AIS).** Let  $U_0$  be some appropriately chosen energy function such that the distribution proportional to  $e^{-U_0}$  can be easily sampled. The idea behind Annealed Importance Sampling (AIS) [69] is to continue between  $U_0$  and the target energy function  $U$ . Specifically, let  $c(t) : [0, 1] \rightarrow [0, 1]$  be some strictly monotone function with  $c(0) = 0$  and  $c(1) = 1$ . Also, let  $(L - 1)$  denote the number of intermediate energy functions between  $U_0$  and  $U$ . For  $1 \leq l \leq L - 1$ , the  $l$ -th intermediate energy  $U_l$  is defined as:

$$(2.1) \quad U_l(s) := \left(1 - c\left(\frac{l}{L}\right)\right)U_0(s) + c\left(\frac{l}{L}\right)U(s).$$

One typical example of  $c$  used in practice is  $c(t) = t$ . Furthermore, for  $1 \leq l \leq L - 1$ , we assume that each distribution  $p_l(\cdot) \propto e^{-U_l(\cdot)}$  is associated with a transition kernel  $T_l(\cdot, \cdot)$  satisfying the detailed balance condition, i.e.,

$$(2.2) \quad p_l(x)T_l(x, y) = p_l(y)T_l(y, x).$$

Using the building blocks given above, AIS follows the procedure described in Algorithm 2.1 to obtain independent weighted samples from each  $p_l$  step by step. Note that we use the symbol  $\propto$  in (2.3) to hide the normalization constant, which remains the same for all independent samples generated by AIS.

Compared to classical MCMC methods, which need to be run over an infinite time horizon to converge to the desired invariant distribution, one advantage of AIS is that it is implemented over a finite time horizon. However, one tradeoff is that the samples need to be reweighted. To examine why reweighting is crucial here, we will show that the distribution of the output configuration  $s$  reweighted by  $w_s$  is exactly the target distribution  $p(s) \propto e^{-U(s)}$ .

Consider the path  $(s_{\frac{1}{2}}, \dots, s_{L-\frac{1}{2}})$  in Algorithm 2.1, which is generated with probability  $p_0(s_{\frac{1}{2}})T_1(s_{\frac{1}{2}}, s_{\frac{3}{2}}) \cdots T_{L-1}(s_{L-\frac{3}{2}}, s_{L-\frac{1}{2}})$ . Multiplying this probability by  $w_s$  given in (2.3) and

**Algorithm 2.1** Annealed Importance Sampling (AIS)

**Initialization:** initial configuration  $s_{\frac{1}{2}}$  sampled from  $p_0(s) \propto e^{-U_0(s)}$ .

**for**  $l = 1 : (L - 1)$  **do**

Take one step (or a few steps) of the transition kernel  $T_l(\cdot, \cdot)$  associated with the distribution  $p_l$  from  $s_{l-\frac{1}{2}}$ . Let  $s_{l+\frac{1}{2}}$  be the resulting configuration.

**end for**

Set  $s := s_{L-\frac{1}{2}}$ .

Compute the associated weight

$$(2.3) \quad w_s = \frac{p_1(s_{\frac{1}{2}})}{p_0(s_{\frac{1}{2}})} \cdots \frac{p_L(s_{L-\frac{1}{2}})}{p_{L-1}(s_{L-\frac{1}{2}})} \propto \frac{e^{-U_1(s_{\frac{1}{2}})}}{e^{-U_0(s_{\frac{1}{2}})}} \cdots \frac{e^{-U_L(s_{L-\frac{1}{2}})}}{e^{-U_{L-1}(s_{L-\frac{1}{2}})}}.$$

**return**  $(s, w_s)$

plugging in the detailed balance condition (2.2) imply that

$$\begin{aligned} & p_0(s_{\frac{1}{2}}) T_1(s_{\frac{1}{2}}, s_{\frac{3}{2}}) \cdots T_{L-1}(s_{L-\frac{3}{2}}, s_{L-\frac{1}{2}}) \cdot \frac{p_1(s_{\frac{1}{2}})}{p_0(s_{\frac{1}{2}})} \cdots \frac{p_L(s_{L-\frac{1}{2}})}{p_{L-1}(s_{L-\frac{1}{2}})} \\ &= p_L(s_{L-\frac{1}{2}}) T_{L-1}(s_{L-\frac{1}{2}}, s_{L-\frac{3}{2}}) \cdots T_1(s_{\frac{3}{2}}, s_{\frac{1}{2}}), \end{aligned}$$

which is equal to the probability of going backward from  $s_{L-\frac{1}{2}}$  to  $s_{\frac{1}{2}}$ . By taking the marginal distribution of  $s_{L-\frac{1}{2}}$  on both sides above, we obtain that the distribution of the output  $s = s_{L-\frac{1}{2}}$  with weight  $w_s$  is exactly  $p_L(\cdot) = p(\cdot) \propto e^{-U(\cdot)}$ .

An alternative way to understand the reweighting in AIS is to use path integral under the continuum limit  $L \rightarrow \infty$ . Consider the task of sampling from some continuous distribution. Let  $U_t(x) := (1 - c(t))U_0(x) + c(t)U(x)$  be the corresponding time-dependent energy annealing between the two energy functions  $U_0, U : \mathbb{R}^d \rightarrow \mathbb{R}$ , where  $t \in [0, 1]$  is a continuous variable. For any  $t \in [0, 1]$ , we pick the transition kernel  $T_t(\cdot, \cdot)$  to be the overdamped Langevin dynamics associated with  $U_t(\cdot)$ . Given the conditions specified above, we can deduce that under the continuum limit, the dynamics of any sample generated by AIS are governed by the following stochastic differential equation (SDE):

$$(2.4) \quad \dot{x} = -\nabla_x U_t(x) + \sqrt{2}\dot{W},$$

where  $W$  above denotes the standard Brownian motion in  $\mathbb{R}^d$ . Under the dynamics (2.4), the logarithm of the probability of a specific continuous path  $\{x(t)\}_{t \in [0, 1]}$  is proportional to

$$(2.5) \quad -U_0(x(0)) - \frac{1}{2} \int_0^1 \dot{W}^2 dt = -U_0(x(0)) - \frac{1}{4} \int_0^1 (\dot{x} + \nabla_x U_t(x))^2 dt.$$

Note that above the normalizing constants are omitted. Moreover, since the reversed dynamics of (2.4) is given by  $\dot{x} = \nabla_x U_t(x) + \sqrt{2}\dot{W}$ , we can deduce that the logarithm of the

probability that going backward from  $x(1)$  to  $x(0)$  along the same path is proportional to

$$(2.6) \quad -U(x(1)) - \frac{1}{2} \int_0^1 \dot{W}^2 dt = -U(x(1)) - \frac{1}{4} \int_0^1 (\dot{x} - \nabla_x U_t(x))^2 dt.$$

Comparing (2.5) with (2.6), we note that one of the two probabilities has to be reweighted in order for them to have the same marginal distribution with respect to  $x(1)$ . As the normalizing constants omitted in (2.5) and (2.6) are all independent of the path  $\{x(t)\}_{t \in [0,1]}$ , we may add (2.5) by some weight  $w$  and equate the sum to (2.6), which is equivalent to reweighting the corresponding probability by  $e^w$ . Then, we may express the weight  $w$  as follows:

$$(2.7) \quad w = U_0(x(0)) - U(x(1)) + \frac{1}{4} \int_0^1 (\dot{x} + \nabla_x U_t(x))^2 dt - \frac{1}{4} \int_0^1 (\dot{x} - \nabla_x U_t(x))^2 dt.$$

Simplifying (2.7) above yields  $w = -\int_0^1 \frac{\partial}{\partial t} U_t(x) dt$ , where the detailed derivation is deferred to Appendix A. Under the limit  $L \rightarrow \infty$ , we note that the logarithm of the weight  $w_s$  given in (2.3) does converge to  $w$ .

**Remark 2.1.** Generally, the weight  $w := w(\tau)$  can be treated as a time-dependent variable satisfying the relation  $w(\tau) = -\int_0^\tau \frac{\partial}{\partial t} U_t(x) dt$  for any  $\tau \in (0, 1)$ . In fact, at any fixed time  $\tau \in (0, 1)$ , the distribution of a sample generated by AIS always deviates from the target distribution  $p_\tau \propto e^{-U_\tau(\cdot)}$ , which results in the necessity of reweighting the distribution of  $x(\tau)$  by  $e^{w(\tau)}$  to correct the bias induced by the deviation. Such deviation between the sampling and target distribution originates from the difference between their normalizing constants, which are often referred to as the free energies in the physics literature [48]. More generally, for any two distributions connected by some fixed continuous-time dynamics, the Jarzynski Equality (JE) [40] was established to pinpoint the relation between their normalizing constants in non-equilibrium thermodynamics. Hence, AIS can also be thought of as a discrete version of JE, and it is sometimes referred to as sampling via JE in other work [8].

**Remark 2.2.** Assuming that the Markov chain associated with  $T_l$  mixes perfectly for every  $l$ , i.e., each  $T_l$  returns an independent sample  $s_{l+\frac{1}{2}}$  from the intermediate distribution  $p_l \propto e^{-U_l(\cdot)}$ , [70] has shown that the smaller the variance of the weight  $w_s$  is, the more efficient AIS will be. To control the variance of the weight, [8, 87] have developed a variant of AIS by combining it with the Sequential Monte Carlo (SMC) method [15], which removes particles with smaller weights and duplicates particles with larger weights via resampling for each  $p_l$ . An alternative way to perform such global moves of the particles based on their weights has been proposed in [59], which utilizes the birth-death process. The evolution of the logarithm of weights used in the birth-death process is given by  $\dot{w} = -\frac{\partial}{\partial t} U_t(x) + \int_{\mathbb{R}^d} \frac{\partial}{\partial t} U_t(x) dx' = 0$ . In contrast, the dynamics of the logarithm of the weights is given by  $\dot{w} = -\frac{\partial}{\partial t} U_t(x)$  for standard AIS, as we have shown above. Comparing the two dynamics illustrates why reweighting is necessary for standard AIS but not needed for algorithms using the birth-death process.

**2.2. Population-Based Monte Carlo Methods.** Instead of keeping track of only one sample, population-based Monte Carlo methods keep track of multiple samples  $\{x_i\}_{i=1}^N$  with invariant distribution  $f(x_1, x_2, \dots, x_N) = \prod_{i=1}^N f_i(x_i)$ , where the target distribution  $p(\cdot) \propto e^{-U(\cdot)}$



coincides with  $f_i(\cdot)$  for at least one  $i \in \{1, 2, \dots, N\}$ . In general, compared to MCMC methods using a single chain, population-based methods take advantage of the interaction between different particles, which encourages the particles to explore different modes of the target distribution in practice.

Among all the population-based methods, one well-known example is the Evolutionary Monte Carlo (EMC) [46, 47]. In the following two subsections, we provide a review of the snooker algorithm [32], and the genetic algorithm [37], which are two important building blocks of EMC. For both algorithms, we set the number of iterations to be  $N$  such that one sample is updated in each iteration. For any  $0 \leq t \leq N$ , we use  $\mathbf{X}^{(t)} = \{x_i^{(t)}\}_{i=1}^N$  to denote the ensemble kept by both algorithms at the  $t$ -th iteration. Moreover, for any  $0 \leq t \leq N$  and subset  $\mathcal{S} \subset \{1, 2, \dots, N\}$ , we let  $\mathbf{X}_{-\mathcal{S}}^{(t)} := \{x_j^{(t)}\}_{j=1}^N \setminus \{x_i^{(t)}\}_{i \in \mathcal{S}}$  be the subset formed by removing the samples  $\{x_i^{(t)}\}_{i \in \mathcal{S}}$  from the ensemble  $\mathbf{X}^{(t)}$ .

**2.2.1. Snooker Algorithm.** Consider the task of sampling from a continuous distribution  $p(\cdot)$  proportional to  $e^{-U(\cdot)}$ , where  $U : \mathbb{R}^d \rightarrow \mathbb{R}$ . The snooker algorithm follows the procedure described in Algorithm 2.2 to update one sample in each iteration. We note that for the empirical distribution formed by the ensemble to converge to the target distribution, Algorithm 2.2 often needs to be repeated multiple times. Regarding the correctness of the snooker algorithm, it suffices to show that the algorithm generates independently and identically distributed samples from the target distribution  $p(\cdot)$  when it reaches equilibrium. Assuming that  $\mathbf{X}^{(t-1)}$  are independently and identically distributed samples from  $p(\cdot)$  for any fixed  $t$ , we only need to prove that the sample  $y$  generated in step (III) of the iteration above is distributed as  $p(\cdot) \propto e^{-U(\cdot)}$  and independent of  $x_k^{(t-1)}$  for any  $k \neq i$ . Such a claim follows directly from Lemma 2.3, which was proved in [52].

---

**Algorithm 2.2** Snooker Algorithm

---

**Initialization:** chosen particle  $x_l$ ; initialized ensemble  $\mathbf{X}^{(I)} = \{x_i\}_{i=1}^N$ ; target distribution  $p(\cdot) \propto e^{-U(\cdot)}$ .

(I) Sample one other particle  $x_j$  uniformly at random from the remaining particles  $\mathbf{X}_{-\{l\}}^{(I)}$  and form the update direction  $e = x_l - x_j$ .

(III) Sample  $r \in \mathbb{R}$  from the following density  $\rho(r)$ :

$$(2.8) \quad \rho(r) \propto |r|^{d-1} p(x_j + re) = |r|^{d-1} p((1-r)x_j + rx_l),$$

where  $p(\cdot)$  above is the target distribution. Compute the new sample  $y = x_j + re$ .

(IV) Form the new ensemble  $\mathbf{X}^{(N)}$  by replacing  $x_l$  with  $y$ , i.e., set  $\mathbf{X}^{(N)} := \mathbf{X}_{-\{l\}}^{(I)} \cup \{y\}$ .

**return**  $\mathbf{X}^{(N)}$

---

**Lemma 2.3.** Fix some probability distribution function  $\pi : \mathbb{R}^d \rightarrow \mathbb{R}$  and some point  $b \in \mathbb{R}^d$ . Assume that  $a \in \mathbb{R}^d$  is distributed as  $\pi(\cdot)$  and let  $e_a := a - b$ . Furthermore, assume that  $r \in \mathbb{R}$  is sampled from the distribution  $\rho(r) \propto |r|^{d-1} \pi(b + re_a)$ , then  $c := b + re_a$  is also distributed as  $\pi(\cdot)$ . Moreover, if  $b$  is independent of  $a$ , then  $c$  is also independent of  $a$ .

We note that it might be hard to sample from the density given in (2.8) directly. Hence, one may also replace step (III) in the for loop with one or a few steps of the Metropolis-Hastings (MH) algorithm for practical use. One other approach is to utilize the stretch move proposed in [34], which emphasizes affine invariance. Specifically, one may sample the scalar  $r$  from some prescribed distribution  $g(\cdot)$  satisfying the symmetry condition  $g(\frac{1}{z}) = zg(z)$ , compute the corresponding new sample  $y = (1 - r)x_j^{(t-1)} + rx_t^{(t-1)}$  and accept the move  $x_t^{(t-1)} \rightarrow y$  with the following probability:

$$(2.9) \quad \min \left\{ 1, \frac{\|y - x_j^{(t-1)}\|^{d-1} \cdot p(y)}{\|x_t^{(t-1)} - x_j^{(t-1)}\|^{d-1} \cdot p(x_t^{(t-1)})} \right\}.$$

**2.2.2. Genetic Algorithm.** Consider the task of sampling from a discrete distribution  $p(\cdot)$  proportional to  $e^{-U(\cdot)}$ , where  $U : \{-1, 1\}^d \rightarrow \mathbb{R}$ . The genetic algorithm we discuss here is motivated by the crossover operation between chromosome pairs in biology. Roughly speaking, in each iteration, a pair of samples' coordinates get mixed according to some crossover operator, which generates a pair of "offsprings". Specifically, the genetic algorithm follows the steps listed in Algorithm 2.3 to obtain samples from  $p(\cdot)$ . Similar to the snooker algorithm, the genetic algorithm also needs to be run multiple times to converge to equilibrium in practice. The correctness of the genetic algorithm can be verified via the fact that the transition probability given in (2.10) satisfies the detailed balance condition with invariant distribution  $\rho(x, y) := p(x)p(y)$ .

---

**Algorithm 2.3** Genetic Algorithm

---

**Initialization:** chosen particle  $x_l = (x_{l,1}, x_{l,2}, \dots, x_{l,d})$ ; initialized ensemble  $\mathbf{X}^{(I)} = \{x_i\}_{i=1}^N$ ; target distribution  $p(\cdot) \propto e^{-U(\cdot)}$ .

- (I) Sample one other particle  $x_j = (x_{j,1}, x_{j,2}, \dots, x_{j,d})$  from  $\mathbf{X}_{-\{j\}}^{(I)}$  uniformly at random.
- (II) Mix the  $2d$  coordinates of  $x_l$  and  $x_j$  to generate two new samples  $y_l = (y_{l,1}, y_{l,2}, \dots, y_{l,d})$  and  $y_j = (y_{j,1}, y_{j,2}, \dots, y_{j,d})$ , such that for any  $1 \leq s \leq d$ ,  $y_{l,s}$  is uniformly sampled from  $\{x_{l,s}, x_{j,s}\}$  and  $y_{j,s}$  is assigned to the remaining coordinate, i.e.,

$$\mathbb{P}(x_{l,s} = y_{l,s}, x_{j,s} = y_{j,s}) = \mathbb{P}(x_{l,s} = y_{j,s}, x_{j,s} = y_{l,s}) = \frac{1}{2}.$$

- (III) Form the new ensemble  $\mathbf{X}^{(N)}$  by replacing  $\{x_l, x_j\}$  with  $\{y_l, y_j\}$ , i.e., set  $\mathbf{X}^{(N)} := \mathbf{X}_{-\{l,j\}}^{(I)} \cup \{y_l, y_j\}$ , with the following acceptance ratio:

$$(2.10) \quad \min \left\{ 1, \frac{p(y_l)p(y_j)}{p(x_l)p(x_j)} \right\} = \min \left\{ 1, \frac{e^{-U(y_l)}e^{-U(y_j)}}{e^{-U(x_l)}e^{-U(x_j)}} \right\}.$$

Set  $\mathbf{X}^{(N)} = \mathbf{X}^{(I)}$  if the move  $\{x_l, x_j\} \rightarrow \{y_l, y_j\}$  above is rejected.  
**return**  $\mathbf{X}^{(N)}$

---



**3. Ensemble-Based Annealed Importance Sampling (AIS).** This section describes how we develop two hybrid algorithms for sampling both continuous and discrete distributions via combining AIS with population-based Monte Carlo methods. Specifically, the first subsection depicts the two hybrid algorithms, while the second subsection considers the case of sampling from a continuous distribution and provides a rigorous derivation of the PDE governing the dynamics of the density tracked by the hybrid algorithm under the continuous time and mean-field limit.

**3.1. Two Hybrid Algorithms.** To improve the efficiency of AIS, there are two questions to be addressed. One question is how to control the variance of the importance weights, while the other one is how to accelerate the mixing of the Markov chain  $T_l$  associated with each intermediate distribution  $p_l$ . The first question is already resolved by combining AIS with SMC and the birth-death process [8, 87]. The second question, however, is the same as improving the efficiency of an arbitrary MCMC algorithm, which consists of three subtasks. The first subtask is to globally explore the entire state space to find all the modes, the second subtask is to exploit each high-probability mode locally, and the third subtask is to balance the weights of the sampling distribution in different modes. For a more detailed description of these three subtasks, one may refer to the introduction of [89].

Note that [8, 59] have already used the birth-death process to handle the reweighting issue described in the third subtask above. Hence, to speed up the convergence of each Markov chain  $T_l$ , we need to resolve the first two subtasks by designing each  $T_l$  in a way that not only explores globally but also exploits locally. As local exploitation can be easily achieved by using any MCMC algorithm, the key problem is how to encourage global exploration. One natural idea is to introduce multiple samplers and make use of the interaction between them. To the best of our knowledge, our work is the first to improve AIS by combining it with some other algorithm that encourages exploration of the whole state space.

For the task of sampling continuous distributions, each  $T_l$  is picked to be a composition of the Unadjusted Langevin Algorithm (ULA) and the snooker algorithm described in Algorithm 2.2 above, where the ULA exploits locally, and the snooker algorithm explores globally. In practice, one may also replace ULA with the Metropolis-Adjusted Langevin Algorithm (MALA) and set each  $T_l$  to be a combination of multiple steps of MALA and the snooker algorithm. Moreover, we use a similar procedure as that of [59] to implement the birth-death dynamics, which adjusts the weights of the particles returned by each  $T_l$ . With all the building blocks specified above, we provide a detailed description of the Ensembled-Based AIS for sampling continuous distributions in Algorithm 3.1.

For the task of sampling discrete distributions, each  $T_l$  is selected to be a composition of the Glauber dynamics [33] and the genetic algorithm depicted in Algorithm 2.3, where the Glauber dynamics exploit locally, and the genetic algorithm explores globally. For practical use, each  $T_l$  may also be chosen to be a combination of multiple steps of Glauber dynamics and the genetic algorithm. Again, we use the birth-death dynamics to balance the particles' weights. Combining all the building blocks listed above gives us the ensembled-based AIS for sampling discrete distributions, whose detailed description is given in Algorithm 3.2.

*Remark 3.1.* Since each  $T_l$  can be picked to be an arbitrary Markov chain with invariant distribution  $p_l$ , we can obtain a truncated version of Algorithm 3.1 by removing the Snooker

Algorithm and keeping the other two parts. Similarly, a truncated form of Algorithm 3.2 can be obtained by removing the Genetic Algorithm in each iteration. Throughout this article, these two truncated algorithms will be referred to as ensemble-based AIS without exploration.

---

**Algorithm 3.1** Ensemble-Based AIS with Exploration for Continuous Distributions
 

---

**Initialization:** number of intermediate distributions  $L$  and time stepsize  $\Delta t = \frac{1}{L}$ ; intermediate distributions  $p_l(\cdot) \propto e^{-U_l(\cdot)}$ , where  $U_l(\cdot) = \left(1 - c(l\Delta t)\right)U_0(\cdot) + c(l\Delta t)U(\cdot)$  ( $1 \leq l \leq L - 1$ ); an initial ensemble of particles  $\mathbf{X}^{(0)} = \{x_i^{(0)}\}_{i=1}^N$  sampled identically and independently from  $p_0(\cdot) \propto e^{-U_0(\cdot)}$ .

**for**  $l = 1 : L$  **do**

**for**  $i = 1 : N$  **do**

**Langevin Dynamics:**

    Update  $x_i^{(l-1+\frac{3i-2}{3N})} = x_i^{(l-1+\frac{i-1}{N})} - \Delta t \nabla U_l(x_i^{(l-1+\frac{i-1}{N})}) + \sqrt{2\Delta t} \xi_i$ , where  $\xi_i$  ( $1 \leq i \leq N$ ) are identically and independently sampled from  $\mathcal{N}(\mathbf{0}, \mathbf{I}_d)$ . Keep all the other particles unchanged by setting  $x_j^{(l-1+\frac{3i-2}{3N})} = x_j^{(l-1+\frac{i-1}{N})}$  ( $j \neq i$ ).

**Snooker Algorithm:**

    Apply Algorithm 2.2 with the chosen particle being  $x_i^{(l-1+\frac{3i-2}{3N})}$ , the initialized ensemble being  $\mathbf{X}^{(l-1+\frac{3i-2}{3N})} = \{x_j^{(l-1+\frac{3j-2}{3N})}\}_{j=1}^N$  and the target density being  $p_l(\cdot) \propto e^{-U_l(\cdot)}$ . Let  $\mathbf{X}^{(l-1+\frac{3i-1}{3N})} = \{x_j^{(l-1+\frac{3i-1}{3N})}\}_{j=1}^N$  be the returned ensemble.

**Birth-Death Dynamics:**

    Compute  $\beta_j^{(l)} := c'(l\Delta t) \left( U(x_j^{(l-1+\frac{3i-1}{3N})}) - U_0(x_j^{(l-1+\frac{3i-1}{3N})}) \right)$  ( $1 \leq j \leq N$ ) and the mean value  $\bar{\beta}^{(l)} := \frac{1}{N} \sum_{j=1}^N \beta_j^{(l)}$ .

**if**  $\beta_i^{(l)} > \bar{\beta}^{(l)}$  **then**

      Kill  $x_i^{(l-1+\frac{3i-1}{3N})}$  with probability  $1 - e^{-(\beta_i^{(l)} - \bar{\beta}^{(l)})\Delta t}$ .

      Duplicate a particle uniformly chosen from the other ones.

**else**

      Duplicate  $x_i^{(l-1+\frac{3i-1}{3N})}$  with probability  $1 - e^{(\beta_i^{(l)} - \bar{\beta}^{(l)})\Delta t}$ .

      Kill a particle uniformly chosen from the other ones.

**end if**

    Denote the updated ensemble by  $\mathbf{X}^{(l-1+\frac{i}{N})} = \{x_j^{(l-1+\frac{i}{N})}\}_{j=1}^N$ .

**end for**

**end for**

**return**  $\mathbf{X}^{(L)} = \{x_i^{(L)}\}_{i=1}^N$ .

---

**Algorithm 3.2** Ensemble-Based AIS with Exploration for Discrete Distributions

**Initialization:** number of intermediate distributions  $L$  and time stepsize  $\Delta t = \frac{1}{L}$ ; intermediate distributions  $p_l(\cdot) \propto e^{-U_l(\cdot)}$ , where  $U_l(\cdot) = \left(1 - c(l\Delta t)\right)U_0(\cdot) + c(l\Delta t)U(\cdot)$  ( $1 \leq l \leq L - 1$ ); an initial ensemble of particles  $\mathbf{X}^{(0)} = \{x_i^{(0)}\}_{i=1}^N$  sampled identically and independently from  $p_0(\cdot) \propto e^{-U_0(\cdot)}$ .

**for**  $l = 1 : L$  **do**

**for**  $i = 1 : N$  **do**

**Glauber Dynamics:**

    Choose a component  $x_{i,j}^{(l-1+\frac{i-1}{N})}$  ( $1 \leq j \leq d$ ) of  $x_i^{(l-1+\frac{i-1}{N})} = (x_{i,1}^{(l-1+\frac{i-1}{N})}, \dots, x_{i,d}^{(l-1+\frac{i-1}{N})})$  uniformly at random and compute  $U_l(x_i^{(l-1+\frac{i-1}{N})})$ .

    Consider the new sample  $y_i^{(l-1+\frac{i-1}{N})}$  formed by flipping the sign of  $x_{i,j}^{(l-1)}$ , i.e.,

$$y_i^{(l-1+\frac{i-1}{N})} = (x_{i,1}^{(l-1+\frac{i-1}{N})}, \dots, x_{i,j-1}^{(l-1+\frac{i-1}{N})}, -x_{i,j}^{(l-1+\frac{i-1}{N})}, x_{i,j+1}^{(l-1+\frac{i-1}{N})}, \dots, x_{i,d}^{(l-1+\frac{i-1}{N})})$$

    and compute  $U_l(y_i^{(l-1+\frac{i-1}{N})})$ .

    Update  $x_i^{(l-1+\frac{3i-2}{3N})}$  to be  $y_i^{(l-1+\frac{i-1}{N})}$  with acceptance ratio  $r$  defined as

$$r := \frac{e^{-U_l(y_i^{(l-1+\frac{i-1}{N})})}}{e^{-U_l(x_i^{(l-1+\frac{i-1}{N})})} + e^{-U_l(y_i^{(l-1+\frac{i-1}{N})})}}.$$

Set  $x_i^{(l-1+\frac{3i-2}{3N})}$  to be  $x_i^{(l-1+\frac{i-1}{N})}$  if the move  $x_i^{(l-1+\frac{i-1}{N})} \rightarrow y_i^{(l-1+\frac{i-1}{N})}$  is rejected. Keep all the other particles unchanged by setting  $x_l^{(l-1+\frac{3i-2}{3N})} = x_l^{(l-1+\frac{i-1}{N})}$  ( $l \neq i$ ).

**Genetic Algorithm:**

  Apply Algorithm 2.3 with the chosen particle being  $x_i^{(l-1+\frac{3i-2}{3N})}$ , the initialized ensemble being  $\mathbf{X}^{(l-1+\frac{3i-2}{3N})} = \{x_j^{(l-1+\frac{3i-2}{3N})}\}_{j=1}^N$  and the target density being  $p_l(\cdot) \propto e^{-U_l(\cdot)}$ . Let  $\mathbf{X}^{(l-1+\frac{3i-1}{3N})} = \{x_j^{(l-1+\frac{3i-1}{3N})}\}_{j=1}^N$  be the returned ensemble.

**Birth-Death Dynamics:**

  Compute  $\beta_j^{(l)} := c'(l\Delta t) \left( U(x_j^{(l-1+\frac{3i-1}{3N})}) - U_0(x_j^{(l-1+\frac{3i-1}{3N})}) \right)$  ( $1 \leq j \leq N$ ) and the mean value  $\bar{\beta}^{(l)} := \frac{1}{N} \sum_{j=1}^N \beta_j^{(l)}$ .

**if**  $\beta_i^{(l)} > \bar{\beta}^{(l)}$  **then**

    Kill  $x_i^{(l-1+\frac{3i-1}{3N})}$  with probability  $1 - e^{-(\beta_i^{(l)} - \bar{\beta}^{(l)})\Delta t}$ .

    Duplicate a particle uniformly chosen from the other ones.

**else**

    Duplicate  $x_i^{(l-1+\frac{3i-1}{3N})}$  with probability  $1 - e^{(\beta_i^{(l)} - \bar{\beta}^{(l)})\Delta t}$ .

    Kill a particle uniformly chosen from the other ones.

**end if**

  Denote the updated ensemble by  $\mathbf{X}^{(l-1+\frac{i}{N})} = \{x_j^{(l-1+\frac{i}{N})}\}_{j=1}^N$ .

**end for**

**end for**

**return**  $\mathbf{X}^{(L)} = \{x_i^{(L)}\}_{i=1}^N$ .

**3.2. Mean-Field Limit and Convergence Properties.** In this subsection, we provide a mean-field analysis of the ensembled-based AIS with exploration (Algorithm 3.1) under the continuous-time limit.

We start with describing the formulation of Algorithm 3.1 under the continuous-time limit  $\Delta t \rightarrow 0$ . Consider the task of sampling from some fixed continuous distribution  $p(\cdot) \propto e^{-U(\cdot)}$  on  $\mathbb{R}^d$  via ensemble-based AIS with exploration. As  $\Delta t \rightarrow 0$ , we recall that the intermediate distributions are given by  $p_t(\cdot) \propto e^{-U_t(\cdot)}$ , where  $U_t(\cdot) := (1 - c(t))U_0(\cdot) + c(t)U(\cdot)$  for any  $t \in [0, 1]$ . Moreover, whenever the snooker algorithm described in Algorithm 2.2 is used, the stretch move proposed in [34] is used to sample from the density given in (2.8). Specifically, let  $g(\cdot) : \mathbb{R} \rightarrow [0, 1]$  denote some prescribed density function satisfying  $\text{supp}(g) = [\frac{1}{a}, a]$  for some  $a \in (1, \infty)$  and the symmetry condition, i.e.,  $g(\frac{1}{z}) = zg(z)$  for any  $z \in [\frac{1}{a}, a]$ . Furthermore, for any time  $t \in [0, 1]$  and collinear points  $u, v, w \in \mathbb{R}^d$ , where  $w = \lambda u + (1 - \lambda)v$  for some  $\lambda \in \mathbb{R}$ , we represent the acceptance ratio of the move  $u \rightarrow w$  given in (2.9) by some function  $A_t(x, y, \lambda)$  defined as:

$$(3.1) \quad A_t(u, v, \lambda) := \min \left\{ 1, \frac{\|w - v\|^{d-1} \cdot p_t(w)}{\|u - v\|^{d-1} \cdot p_t(u)} \right\} = \min \left\{ 1, |\lambda|^{d-1} \frac{e^{-U_t(\lambda u + (1-\lambda)v)}}{e^{-U_t(u)}} \right\}.$$

We represent the empirical measure formed by the ensemble  $\mathbf{X}^{(t)} := \{x_i^{(t)}\}_{i=1}^N$  by  $\mu_N^{(t)} := \frac{1}{N} \sum_{i=1}^N \delta_{x_i^{(t)}}$  for any time  $t \in [0, 1]$ . Similar to the discrete version presented in Algorithm 3.1, the evolution of the particles in  $\mathbf{X}^{(t)}$  consists of three parts as  $t$  ranges from 0 to 1:

- Each particle  $x_i^{(t)}$  diffuses independently according to the Langevin Dynamics (2.4).
- Each particle  $x_i^{(t)}$  is updated via the stretch move.
- For any  $1 \leq i \leq N$ , each particle  $x_i^{(t)}$  possesses an independent exponential clock with instantaneous birth-death rate

$$(3.2) \quad \beta_i^{(t)} := c'(t) \left( U(x_i^{(t)}) - U_0(x_i^{(t)}) \right) - \frac{1}{N} \sum_{j=1}^N c'(t) \left( U(x_j^{(t)}) - U_0(x_j^{(t)}) \right).$$

Assume that the initial empirical distribution  $\mu_N^{(0)}$  converges to some  $\rho_0$  in law under the large particle limit  $N \rightarrow \infty$ . Then for any  $t \in [0, 1]$ , we can heuristically deduce that  $\mu_N^{(t)}$  converges to some  $\rho_t$  in law as  $N \rightarrow \infty$ , whose evolution is governed by the following PDE with initial condition  $\rho_0(x) = \rho(0, x)$ :

$$(3.3) \quad \begin{aligned} \frac{\partial}{\partial t} \rho(t, x) &= \nabla_x \cdot \left( \left( (1 - c(t)) \nabla_x U_0(x) + c(t) \nabla_x U(x) \right) \rho(t, x) \right) + \Delta_x \rho(t, x) \\ &+ \int_{\frac{1}{a}}^a |\lambda|^{d-2} g(\lambda^{-1}) \left( \int_{\mathbb{R}^d} A_t(\lambda x + (1 - \lambda)y, y, \lambda^{-1}) \rho(t, y) \rho(t, \lambda x + (1 - \lambda)y) dy \right) d\lambda \\ &- \left( \int_{\frac{1}{a}}^a g(\lambda) \left( \int_{\mathbb{R}^d} A_t(x, y, \lambda) \rho(t, y) dy \right) d\lambda \right) \rho(t, x) \\ &- \left( c'(t) \left( U(x) - U_0(x) \right) - \int_{\mathbb{R}^d} c'(t) \left( U(x) - U_0(x) \right) \rho(t, x) dx \right) \rho(t, x). \end{aligned}$$

*Remark 3.2.* For the RHS of the PDE (3.3), the first and second terms correspond to the Langevin dynamics, the third and fourth terms come from the stretch move, while the last term stands for the birth-death process. A complete derivation of the PDE (3.3) is postponed to Appendix B.

**4. Numerical Experiments.** In this section, we exhibit the effectiveness of the ensemble-based AIS with exploration via a series of numerical examples. From the numerical tests presented below, we can see that Algorithm 3.1 and 3.2 outperform both ensemble-based AIS without exploration and standard AIS that involves reweighting, neither of which contains any part encouraging global moves towards the undiscovered modes. The testing cases below are selected based on examples used in previous work [49, 74, 77, 89]. For all the AIS-related algorithms tested in this section, we pick  $c(t) = t : [0, 1] \rightarrow [0, 1]$  to be the function used for interpolating between the starting and the target distribution. All the experiments are conducted via MATLAB R2023b on a laptop with a 2.2 GHz Core Intel i9 processor.

**4.1. Continuous Distributions.** The first subsection focuses on testing Algorithm 3.1 on a few continuous distributions with varying dimensions. To illustrate the efficacy of adding the exploration part, we make a comparison between Algorithm 3.1, ensemble-based AIS without exploration, and standard AIS. Regarding the implementation of Algorithm 3.1, we use the stretch move proposed in [34] to sample from the density (2.8) in the snooker algorithm. Moreover, we use MALA to replace ULA in our implementation of all the algorithms we test. Furthermore, two versions of standard AIS are implemented. One of them uses MALA as the transition kernel, while the other one's transition kernel is selected to be the MH Algorithm associated with a Gaussian proposal density.

Let  $p(x) = \frac{1}{Z}e^{-U(x)}$  denote the target continuous distribution, where  $Z$  is the normalizing constant. Also, we use  $\{s_i\}_{i=1}^N$  and  $\{w_i\}_{i=1}^N$  to denote the samples generated by an algorithm, where the  $\{s_i\}_{i=1}^N$  are the locations and  $\{w_i\}_{i=1}^N$  are the weights. Note that the weights are all equal for ensemble-based AIS algorithms utilizing the birth death dynamics, i.e.,  $w_i = \frac{1}{N}$  ( $1 \leq i \leq N$ ). We take two approaches to evaluate the quality of the empirical distribution  $\hat{p}$  formed by the generated samples  $\{s_i\}_{i=1}^N$  and  $\{w_i\}_{i=1}^N$ . On the one hand, note that the Kullback–Leibler (KL) divergence between  $\hat{p}$  and  $p$  can be explicitly written as

$$\begin{aligned}
 D_{\text{KL}}(\hat{p} \parallel p) &= \int_{\text{supp}(\hat{p})} \hat{p}(x) \log \left( \frac{\hat{p}(x)}{p(x)} \right) dx = \sum_{i=1}^N w_i \log \left( \frac{w_i}{p(s_i)} \right) \\
 (4.1) \quad &= \sum_{i=1}^N w_i \log(w_i) - \sum_{i=1}^N w_i \log \left( \frac{1}{Z} e^{-U(s_i)} \right) \\
 &= \sum_{i=1}^N w_i U(s_i) + \sum_{i=1}^N w_i \log(w_i) - \log(Z).
 \end{aligned}$$

As the normalizing constant  $Z$  is independent of the generated samples and weights, we may drop off the  $-\log(Z)$  term above to obtain the expression of the loss function

$$(4.2) \quad \mathcal{L}_{\text{KL}}(\{w_i\}_{i=1}^N, \{s_i\}_{i=1}^N) = \sum_{i=1}^N w_i U(s_i) + \sum_{i=1}^N w_i \log(w_i).$$

We remark that the loss function is not guaranteed to be always positive since the  $-\log(Z)$  term gets dropped in the expression above. Throughout this subsection, the loss function defined in (4.2) is referred to as the empirical KL loss.

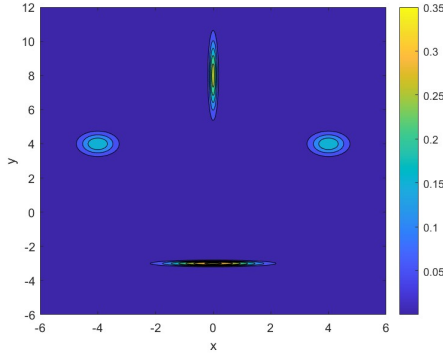
On the other hand, note that the empirical KL loss function is not an ideal metric for identifying the number of modes within the weighted samples. To confirm which algorithms can discover the modes of the underlying distribution more effectively, we also plot the marginal distribution of certain coordinates formed by the samples generated by all four algorithms listed above and make a comparison between the plots.

**4.1.1. Gaussian Mixture Model.** We first test the performance of the four algorithms on a 2-dimensional Gaussian mixture model, which is of similar form as the testing cases used in [59, 60, 89]. Specifically, the target density can be written as

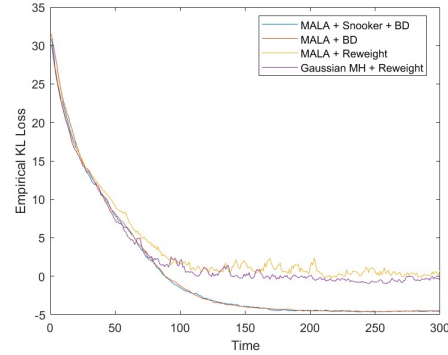
$$(4.3) \quad \pi(x, y) := \sum_{i=1}^4 w_i \mathcal{N}(x, y; \mu_i, \Sigma_i),$$

where  $\mu_i \in \mathbb{R}^2$ ,  $\Sigma_i \in \mathbb{R}^{2 \times 2}$  and  $\mathcal{N}(x, y; \mu_i, \Sigma_i)$  denotes the Gaussian distribution in  $\mathbb{R}^2$  with mean vector  $\mu_i$  and covariance matrix  $\Sigma_i$  for any  $1 \leq i \leq 4$ . The numerical values of the parameters used in our experiment are given by

$$(4.4) \quad \begin{aligned} w_i &= \frac{1}{4} \quad (1 \leq i \leq 4), \quad \mu_1 = [0, -3]^T, \quad \mu_2 = [0, 8]^T, \quad \mu_3 = [-4, 4]^T, \quad \mu_4 = [4, 4]^T \\ \Sigma_1 &= \begin{bmatrix} 1.2 & 0 \\ 0 & 0.01 \end{bmatrix}, \quad \Sigma_2 = \begin{bmatrix} 0.01 & 0 \\ 0 & 2 \end{bmatrix}, \quad \Sigma_3 = \Sigma_4 = \begin{bmatrix} 0.2 & 0 \\ 0 & 0.2 \end{bmatrix}. \end{aligned}$$



(a) Target Density



(b) Empirical KL Loss

Figure 1: (a) Contour plot of the target density in 4.1.1; (b) Plots of  $\mathcal{L}_{\text{KL}}$  evaluated at evolving weighted samples generated by different testing algorithms in 4.1.1.

A contour plot of the target density is provided in Figure (1a). In our implementation, we set the number of samplers and time steps to be  $N = 1000$  and  $L = 300$ , respectively.

Moreover, for the standard AIS using an MH Algorithm as the transition kernel, we pick its Gaussian proposal density to be  $\mathcal{N}(\mathbf{0}, 0.01\mathbf{I}_2)$ . The starting distribution is selected to be the normal distribution  $\mathcal{N}(\mathbf{0}, \mathbf{I}_2)$  in  $\mathbb{R}^2$ . We track values of the empirical KL loss function evaluated at weighted samples generated by the four testing algorithms with respect to time and plot them in Figure (1b). For all the plots included in this paper, we use the abbreviation “BD” in the legends to denote the birth-death dynamics.

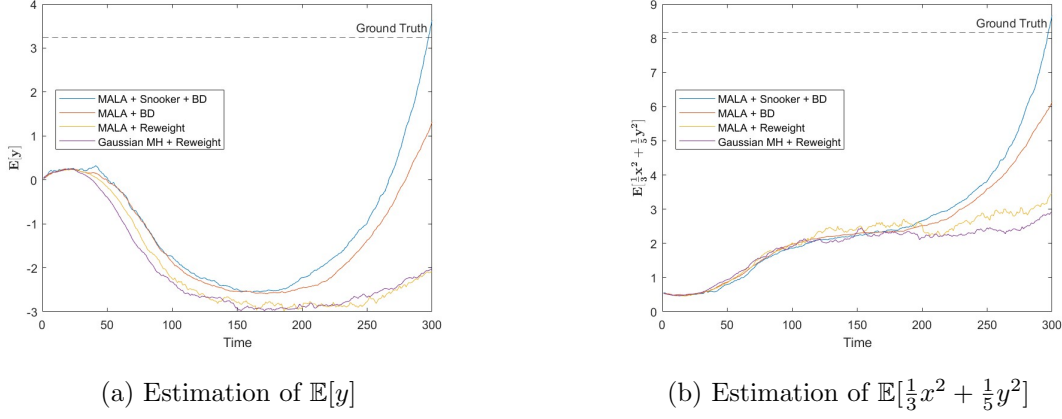


Figure 2: Evolving Estimations of  $\mathbb{E}[f(x, y)]$  evaluated at weighted samples generated by different testing algorithms in 4.1.1 for two different functions  $f_1(x, y) = y$  and  $f_2(x, y) = \frac{1}{3}x^2 + \frac{1}{5}y^2$ .

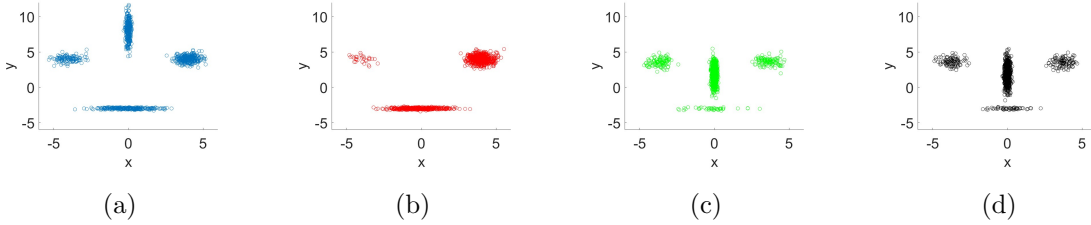


Figure 3: Scatter plots of the empirical samples returned by different testing algorithms in 4.1.1; (a) MALA + Snooker + BD; (b) MALA + BD; (c) MALA + Reweight; (d) Gaussian MH + Reweight.

Our results in Figure (1b) reveal that the two ensemble-based AIS algorithms converge faster and generate better samples than the two standard AIS algorithms in terms of the loss function  $\mathcal{L}_{\text{KL}}$ . For two different test functions  $f_1(x, y) = y$  and  $f_2(x, y) = \frac{x^2}{3} + \frac{y^2}{5}$ , we plot the estimated values of  $\mathbb{E}[f_1]$  and  $\mathbb{E}[f_2]$  given by weighted samples associated with different algorithms. From the two plots given in Figure (2) we can see that Algorithm 3.1 returns much more accurate estimations of the two expectation values than the other three



algorithms. Furthermore, we also provide scattered plots of the empirical samples generated by the four algorithms in Figure (3), from which we can see that only Algorithm 3.1 succeeds in discovering the mode centered around  $\mu_2$ . From all the plots above, we conclude that the exploration part serves as an essential factor for discovering modes and generating samples of higher quality in this example.

**4.1.2. Ginzburg-Landau Distributions.** The Ginzburg-Landau (GL) theory is a mathematical model used in the studies of superconductivity [35, 36]. Here, we consider a continuous distribution coming from a simplified version of the Ginzburg-Landau model in  $\mathbb{R}^d$ , whose associated energy function  $\mathcal{U}$  is defined as

$$(4.5) \quad \mathcal{U}(x(\mathbf{r})) := \int_{\Omega} \left( \frac{\lambda}{2} |\nabla_{\mathbf{r}} x(\mathbf{r})|^2 + \frac{1}{\lambda} V(x(\mathbf{r})) \right) d\mathbf{r},$$

where  $\Omega$  is the domain,  $x = x(\mathbf{r}) : \Omega \rightarrow \mathbb{R}$  is a sufficiently smooth function with Dirichlet boundary condition  $x(\mathbf{r}) = 0$  ( $\forall \mathbf{r} \in \partial\Omega$ ),  $\lambda > 0$  is some fixed parameter and  $V(x) = \frac{1}{4}(1-x^2)^2$  is the potential function.

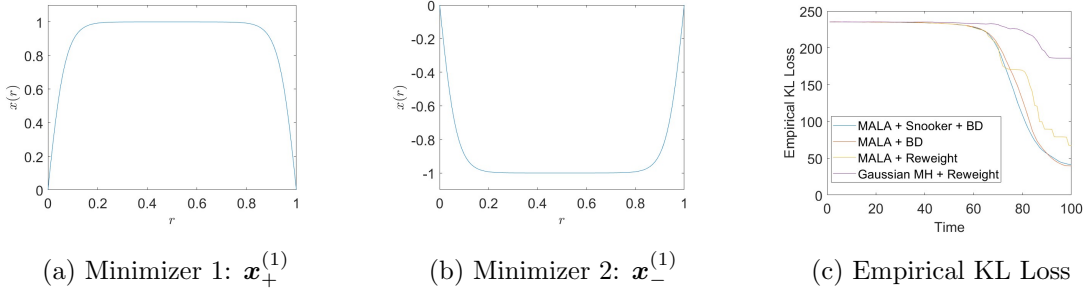


Figure 4: (a) & (b) Two minimizers  $\mathbf{x}_+^{(1)}$  and  $\mathbf{x}_-^{(1)}$  of the 1D Ginzburg-Landau Energy (4.5) with  $\lambda = 0.05$ ; (c) Plots of  $\mathcal{L}_{\text{KL}}$  evaluated at evolving weighted samples generated by different testing algorithms in the 1D case of 4.1.2.

For the first case when  $\Omega = [0, L]$ , the function  $x = x(\mathbf{r})$  is discretized as  $\mathbf{x} := (x_i)_{i=1}^d$  with boundary condition  $x_0 = x_{d+1} = 0$ , which contains the values of the function  $x = x(\mathbf{r})$  on the uniform grid points  $\{ih\}_{i=0}^{d+1}$  with  $h = \frac{L}{d+1}$ . Then, the corresponding discrete approximation of (4.5) is given by

$$(4.6) \quad \mathcal{U}(x(r)) \approx U_1(\mathbf{x}) := \sum_{i=1}^{d+1} \left( \frac{\lambda}{2} \left| \frac{x_i - x_{i-1}}{h} \right|^2 + \frac{1}{4\lambda} (1 - x_i^2)^2 \right).$$

The target distribution is set to be the Boltzmann distribution  $p_1(\mathbf{x}) \propto e^{-\beta U_1(\mathbf{x})}$  associated with (4.6), where  $\beta = \frac{1}{T}$  is the inverse temperature parameter. For our numerical experiments on the 1D case, we choose  $\lambda = 0.05, d = 16, \beta = 3$  and  $L = 1$ . From previous studies [25], we know that  $p_1$  contains two local modes centered around the two local minimizers  $\mathbf{x}_+^{(1)}$

and  $\mathbf{x}_-^{(1)}$  of the 1D GL energy function (4.6), which are plotted in Figure (4a) and (4b) respectively. In our implementation, we pick the number of samplers and time steps to be  $N = 1000$  and  $L = 100$ . Moreover, for the standard AIS whose transition kernel is given by an MH Algorithm, we pick its Gaussian proposal density to be  $\mathcal{N}(\mathbf{0}, 0.01\mathbf{I}_{16})$ . The starting distribution is selected to be the normal distribution  $\mathcal{N}(\mathbf{0}, 0.01\mathbf{I}_{16})$  in  $\mathbb{R}^{16}$ . In order to compare the testing algorithms' abilities to discover modes of the underlying distribution, we also plot the marginal distribution of  $(x_5, x_6)$  for the empirical samples returned by each algorithm, which are exhibited in Figure (5).

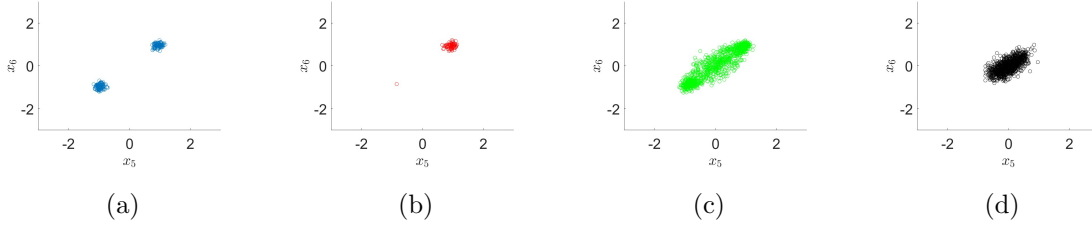


Figure 5: Scatter plots of the marginal distribution at  $(x_5, x_6)$  returned by different testing algorithms in the 1D case of 4.1.2; (a) MALA + Snooker + BD; (b) MALA + BD; (c) MALA + Reweight; (d) Gaussian MH + Reweight.

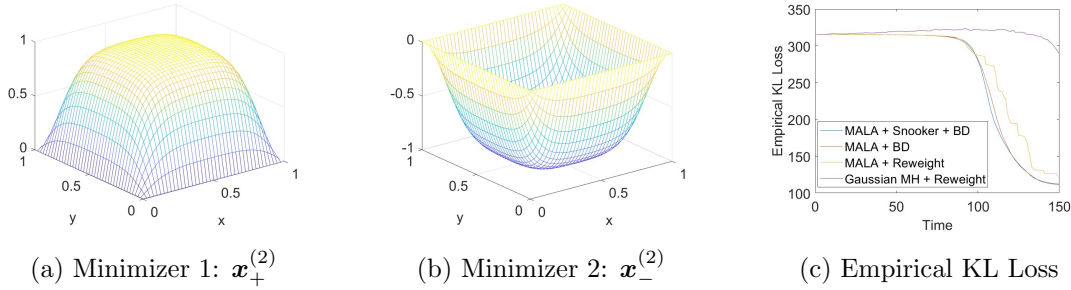


Figure 6: (a) & (b) Two minimizers  $\mathbf{x}_+^{(2)}$  and  $\mathbf{x}_-^{(2)}$  of the 2D Ginzburg-Landau Energy (4.5) with  $\lambda = 0.125$ ; (c) Plots of  $\mathcal{L}_{\text{KL}}$  evaluated at evolving weighted samples generated by different testing algorithms in the 2D case of 4.1.2.

For the second case when  $\Omega = [0, L]^2$ , the function  $x = x(\mathbf{r})$  is discretized as  $\mathbf{x} := (x_{i,j})_{i,j=1}^d$  with boundary condition  $x_{0,k} = x_{k,0} = x_{(d+1),l} = x_{l,(d+1)} = 0$  ( $\forall 0 \leq k, l \leq d+1$ ), which contains the values of the function  $x = x(\mathbf{r})$  on the uniform grid points  $\{(ih, jh)\}_{i,j=0}^{d+1}$  with

$h = \frac{L}{d+1}$ . Then, the corresponding discrete approximation of (4.5) is given by

$$(4.7) \quad \mathcal{U}(x(r)) \approx U_2(\mathbf{x}) := \sum_{i=1}^d \sum_{j=1}^d \left( \frac{\lambda}{4} \left| \frac{x_{i,j} - x_{(i-1),j}}{h} \right|^2 + \frac{\lambda}{4} \left| \frac{x_{i,j} - x_{(i+1),j}}{h} \right|^2 \right. \\ \left. + \frac{\lambda}{4} \left| \frac{x_{i,j} - x_{i,(j-1)}}{h} \right|^2 + \frac{\lambda}{4} \left| \frac{x_{i,j} - x_{i,(j+1)}}{h} \right|^2 + \frac{1}{4\lambda} (1 - x_{i,j}^2)^2 \right).$$

In a similar manner to the 1D case, the target distribution for the 2D case is picked to be the Boltzmann distribution  $p_2(\mathbf{x}) \propto e^{-\beta U_2(\mathbf{x})}$  associated with (4.7), where  $\beta = \frac{1}{T}$  and  $T$  is the temperature. For our numerical experiments on the 2D case, we choose  $\lambda = 0.125, d = 4, \beta = 10$  and  $L = 1$ . Analogously,  $p_2$  contains two local modes centered around the two local minimizers  $\mathbf{x}_+^{(2)}$  and  $\mathbf{x}_-^{(2)}$  of the 2D GL energy function (4.6), which are exhibited in Figure (6a) and (6b) respectively. In our implementation, we pick the number of samplers and time steps to be  $N = 1000$  and  $L = 150$ . For the standard AIS whose transition kernel is given by an MH Algorithm, we pick its Gaussian proposal density to be  $\mathcal{N}(\mathbf{0}, 0.001\mathbf{I}_{16})$ . The starting distribution is selected to be the normal distribution  $\mathcal{N}(\mathbf{0}, 0.01\mathbf{I}_{16})$  in  $\mathbb{R}^{16}$ . Again, we examine the testing algorithms' capabilities of identifying the modes in the target distribution by plotting the marginal distribution of  $(x_5, x_6)$  for the empirical samples returned by each algorithm in Figure (7).

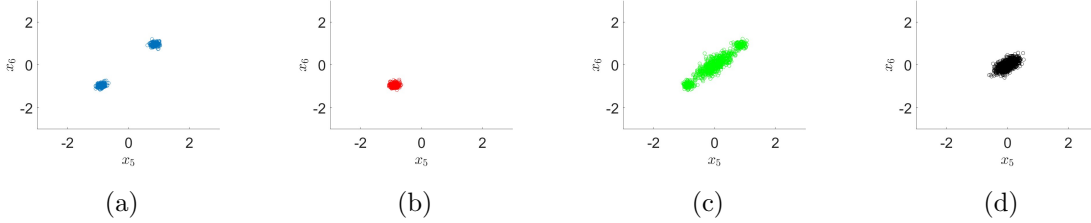


Figure 7: Scatter plots of the marginal distribution at  $(x_5, x_6)$  returned by different testing algorithms in the 2D case of 4.1.2; (a) MALA + Snooker + BD; (b) MALA + BD; (c) MALA + Reweight; (d) Gaussian MH + Reweight.

On the one hand, from the two plots of the empirical KL loss functions above, we find that the two ensemble-based AIS algorithms converge faster and generate samples of higher quality compared to the two standard AIS algorithms when measured under  $\mathcal{L}_{\text{KL}}$ . On the other hand, from the scattered plots of the marginal distributions, we also observe that the Algorithm 3.1 can discover the local modes in a more effective way than the other three algorithms. Both claims above justify that the exploration part can indeed help improve the efficiency of the AIS algorithm.

**4.1.3. Product of Multiple Double Well Distributions.** For the last numerical test on continuous distributions, we choose the target density to be a product of multiple double-well

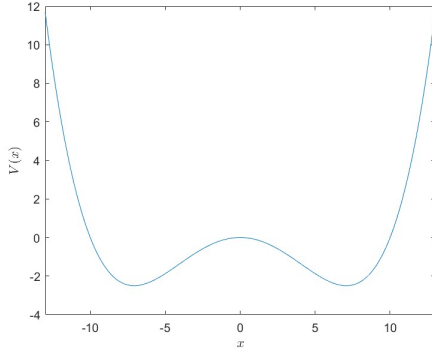
densities in  $\mathbb{R}$ , which is of similar form as one of the testing cases used in [68]. Specifically, we first consider a double-well distribution  $q : \mathbb{R} \rightarrow [0, 1]$  defined as follows

$$(4.8) \quad q(x) \propto \exp(-\beta(x^4 - 100x^2)),$$

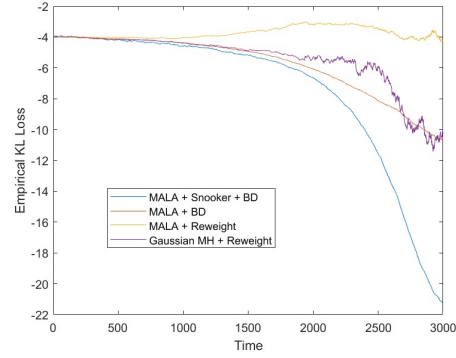
where  $\beta = \frac{1}{T}$  is the inverse of the temperature associated with this model. From (4.8) one can see that  $q(\cdot)$  has two modes centered at  $x_+ = 5\sqrt{2}$  and  $x_- = -5\sqrt{2}$ , respectively. This can also be inferred from the plot of the associated potential function  $V(x) := \beta(x^4 - 100x^2)$  in Figure (8a). The target density function in  $\mathbb{R}^{20}$  is further defined as follows:

$$(4.9) \quad p(\mathbf{x}) = p(x_1, x_2, \dots, x_{20}) \propto \left( \prod_{j=1}^{10} q(x_j) \right) \cdot \left( \prod_{j=11}^{20} \frac{1}{\sqrt{2\pi}} e^{-\frac{1}{2}x_j^2} \right),$$

i.e., the first 10 coordinates are distributed as  $q(\cdot)$  while the last 10 coordinates are distributed as standard normal random variables. Since each  $q(\cdot)$  contains 2 local modes, a direct computation yields that the target density  $p(\cdot)$  has  $2^{10} = 1024$  local modes.



(a) Double-Well Potential Energy  $V(x)$



(b) Empirical KL Loss

Figure 8: (a) Plot of the potential function  $V(x)$  with  $\beta = 0.001$ ; (b) Plots of  $\mathcal{L}_{\text{KL}}$  evaluated at evolving weighted samples generated by different testing algorithms in 4.1.3.

When testing the performance of the four algorithms on this example, which is of relatively higher dimension and contains more local modes, we set the inverse temperature parameter, number of samplers, and time steps to be  $\beta = 0.001$ ,  $N = 3000$  and  $L = 3000$ , respectively. Moreover, for the standard AIS whose transition kernel is given by the MH Algorithm, we choose its Gaussian proposal density to be  $\mathcal{N}(\mathbf{0}, \mathbf{I}_{20})$ . The starting distribution is selected to be the normal distribution  $\mathcal{N}(\mathbf{0}, \mathbf{I}_{20})$  in  $\mathbb{R}^{20}$ . Again, we track values of the empirical KL loss function evaluated at weighted samples generated by the four testing algorithms with respect to time and plot them in Figure (8b). For the purpose of testing the listed algorithms' abilities to discover local modes, we also plot the marginal distribution of  $(x_1, x_2)$  for the empirical samples returned by each algorithm, which are listed in Figure (9).

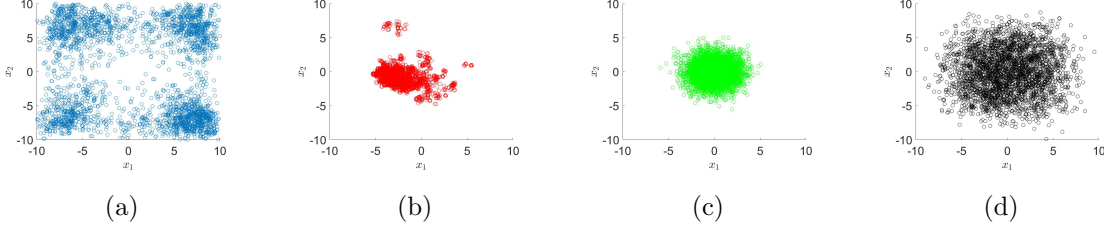


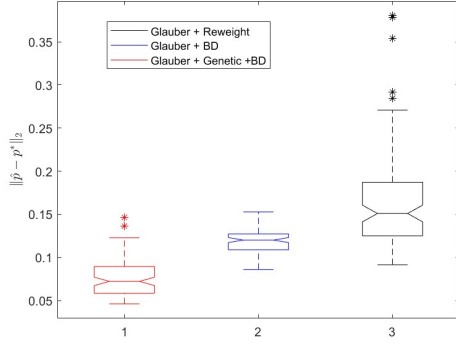
Figure 9: Scatter plots of the marginal distribution at  $(x_1, x_2)$  returned by different testing algorithms in 4.1.3; (a) MALA + Snooker + BD; (b) MALA + BD; (c) MALA + Reweight; (d) Gaussian MH + Reweight.

From the plot of the empirical KL loss functions, we find that Algorithm 3.1 converges faster and generates samples closer to the target distribution than the other three algorithms. More importantly, from the four scattered plots in Figure (9) we can see that only Algorithm 3.1 manages to find all the four local modes  $(\pm 5\sqrt{2}, \pm 5\sqrt{2})$  within the marginal distribution of  $(x_1, x_2)$ , which reveals that the exploration part helps improve the AIS algorithm's ability to discover modes.

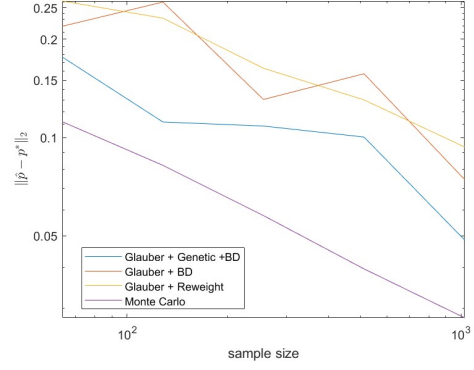
**4.2. Discrete Distributions: Ising Models.** For the case of sampling discrete distributions, we focus on the Ising model, which is a simple but commonly used model in statistical physics. Specifically, we test Algorithm 3.2 on a few one-dimensional and two-dimensional Ising models of similar form as the ones used in [74]. Analogous to the cases of continuous distributions, we also compare Algorithm 3.2 with ensemble-based AIS without exploration and standard AIS to justify the essentiality of the exploration part. For the standard AIS, the transition kernel is picked to be the Glauber dynamics. For any empirical distribution  $\hat{p}$  formed by the samples returned by a testing algorithm, we measure the quality of the samples via the  $L_2$  loss function  $\mathcal{L}_2(\hat{p}, p) = \|\hat{p} - p^*\|_2$ , where  $p^*(\cdot) \propto e^{-U(\cdot)} : \{-1, 1\}^d \rightarrow [0, 1]$  is the target distribution. For each Ising model, we perform three experiments to illustrate the effectiveness of Algorithm 3.2. In the first experiment, we fix the sample size and run each algorithm multiple times to create a box plot of the  $L_2$  loss function's value for each algorithm. For the second experiment, we investigate how the  $L_2$  loss function depends on the sample size for each algorithm, where the standard Monte Carlo method is chosen to be the reference. In the third experiment, we set the sample size to be relatively large and plot the samples generated by Algorithm 3.2.

**4.2.1. 1D Ising Models.** Consider a generalized one-dimensional Ising model, where interaction exists between both the nearest and the second nearest neighbor pairs. The associated distribution  $p(\cdot) : \{-1, 1\}^d \rightarrow [0, 1]$  is defined as

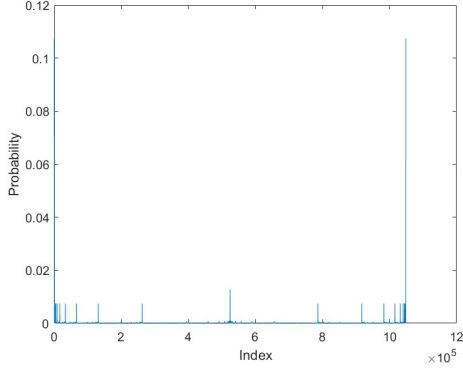
$$(4.10) \quad p(\mathbf{x}) = p(x_1, x_2, \dots, x_d) \propto \exp \left( -\beta \sum_{i=1}^{d-1} J_1 x_i x_{i+1} - \beta \sum_{i=1}^{d-2} J_2 x_i x_{i+2} \right).$$



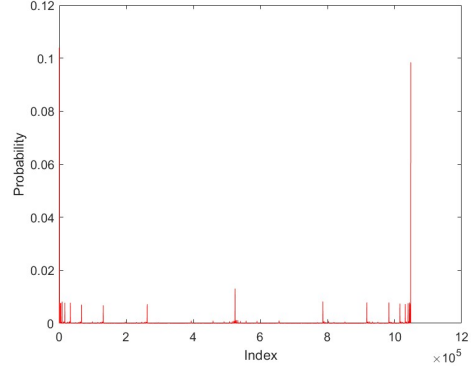
(a) Box plot with fixed sample size



(b) Error plot with varying sample sizes



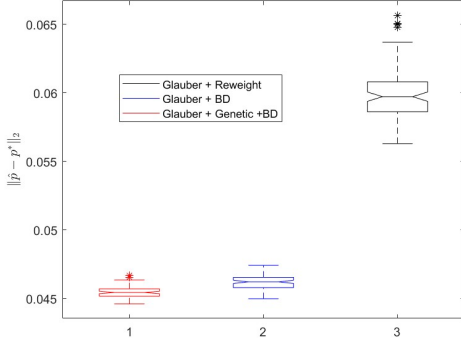
(c) Target Distribution



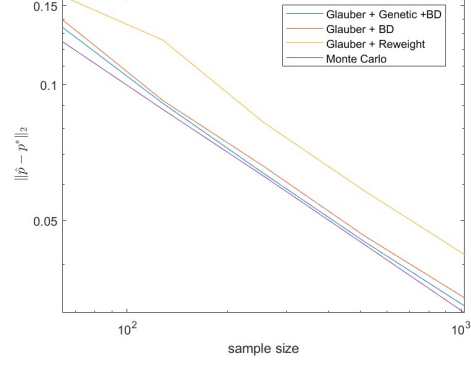
(d) Generated Empirical Distribution

Figure 10: One-dimensional ferromagnetic Ising model with  $\beta = 0.8$  and  $d = 20$ ; (a) Box plot with fixed sample size  $N = 512$ ; (b) Error plot with varying sample sizes  $N \in \{64, 128, 256, 512, 1024\}$ ; (c) Target distribution; (d) Empirical distribution formed by samples generated by Algorithm 3.2 (sample size  $N = 65536$ ).

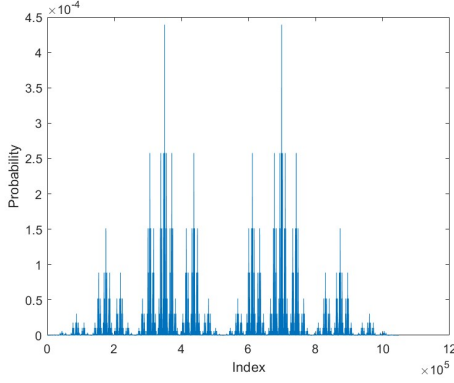
Note that  $\beta = \frac{1}{T}$  in (4.10) is the inverse temperature parameter. In our experiments on the one-dimensional Ising models, we set  $\beta = 0.8$ ,  $d = 20$  and the number of time steps to be  $L = 64$ . The initial distribution is fixed to be the uniform distribution over  $\{-1, 1\}^{20}$ . Moreover, for the experiments producing box plots, we fix the sample size to be  $N = 512$ . For the experiments investigating how the loss function  $\mathcal{L}_2(\hat{p}, p)$  depends on the sample size, we increase the sample size from  $N = 64$  to  $N = 1024$ , doubling it at each round. Finally, when visualizing the empirical distribution formed by the samples generated by Algorithm 3.2, we choose the sample size to be  $N = 65536$ .



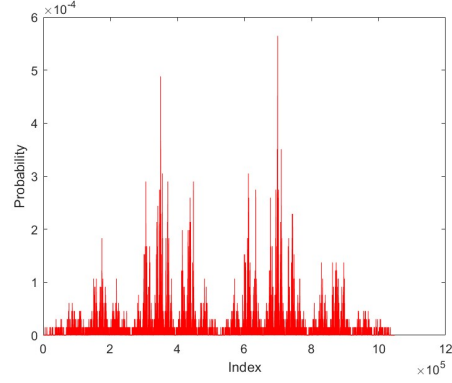
(a) Box plot with fixed sample size



(b) Error plot with varying sample sizes



(c) Target Distribution



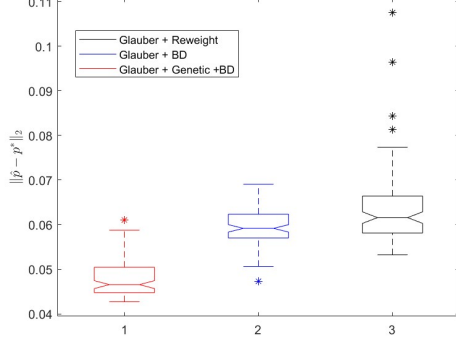
(d) Generated Empirical Distribution

Figure 11: One-dimensional antiferromagnetic Ising model with  $\beta = 0.8$  and  $d = 20$ ; (a) Box plot with fixed sample size  $N = 512$ ; (b) Error plot with varying sample sizes  $N \in \{64, 128, 256, 512, 1024\}$ ; (c) Target distribution; (d) Empirical distribution formed by samples generated by Algorithm 3.2 (sample size  $N = 65536$ ).

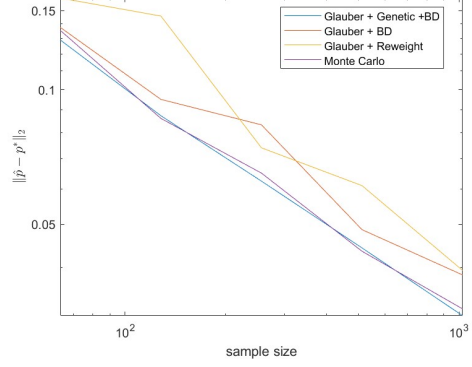
The first model we test is the ferromagnetic one-dimensional Ising model, whose interaction coefficients in (4.10) are given by  $J_1 = -1$  and  $J_2 = -\frac{1}{3}$ . The testing results are listed in Figure 10, from which we can see that Algorithm 3.2 does outperform the ensemble-based AIS without exploration and the standard AIS on the first model. Specifically, the box plots reveal that Algorithm 3.2 returns more accurate samplers than the other two algorithms, while the error plots show that Algorithm 3.2 induces smaller error than the other two algorithms for varying sample sizes. Furthermore, when the sample size is set to be sufficiently large, we observe that the empirical distribution generated by Algorithm 3.2 is reasonably close to the target distributions. The second model we test is the antiferromagnetic Ising model, whose interaction coefficients in (4.10) are given by  $J_1 = 1$  and  $J_2 = \frac{1}{3}$ . The plotted figures are



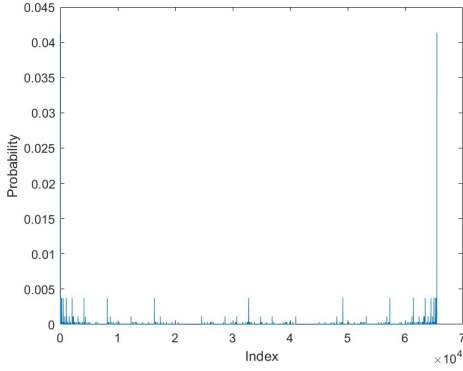
given in Figure (11), where we can infer that Algorithm 3.2 performs better than the other two algorithms on the second model by comparing the sub-figures in Figure (11) in a similar way.



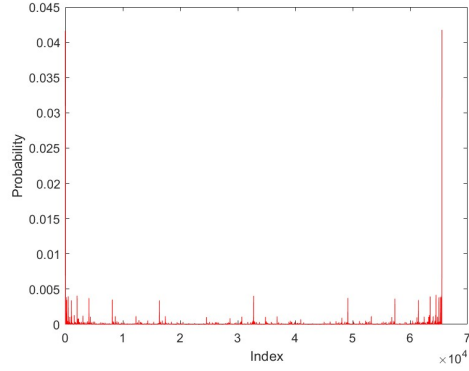
(a) Box plot with fixed sample size



(b) Error plot with varying sample sizes



(c) Target Distribution



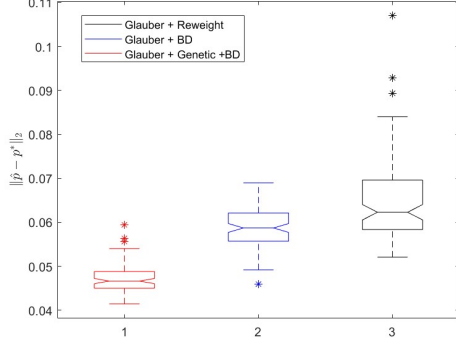
(d) Generated Empirical Distribution

Figure 12: Two-dimensional ferromagnetic Ising model with  $\beta = 0.3$  and  $d = 4$ ; (a) Box plot with fixed sample size  $N = 512$ ; (b) Error plot with varying sample sizes  $N \in \{64, 128, 256, 512, 1024\}$ ; (c) Target distribution; (d) Empirical distribution formed by samples generated by Algorithm 3.2 (sample size  $N = 65536$ ).

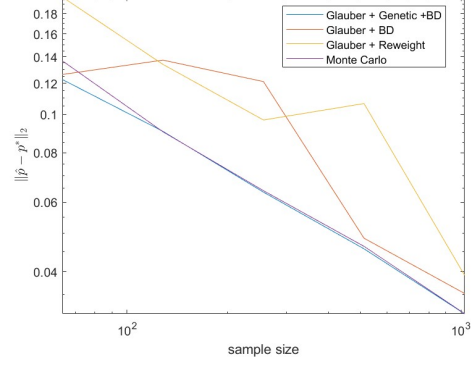
**4.2.2. 2D Ising Models.** We further consider the two-dimensional Ising model with the periodic boundary condition, where interaction exists between only the nearest neighbor pairs. The corresponding distribution  $p(\cdot) : \{-1, 1\}^{d^2} \rightarrow [0, 1]$  can be written as

$$(4.11) \quad p(\mathbf{x}) = p(\{x_{i,j}\}_{i,j=1}^d) \propto \exp\left(-\beta \sum_{i=1}^d \sum_{j=1}^d J(x_{i,j}x_{i+1,j} + x_{i,j}x_{i,j+1})\right),$$

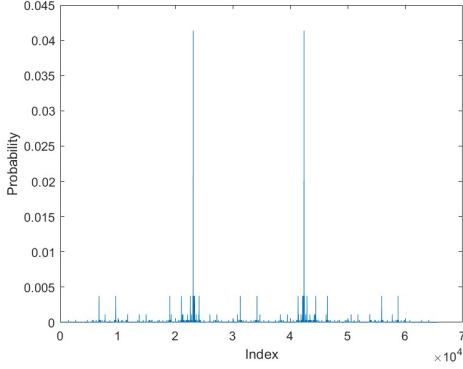
where  $\beta = \frac{1}{T}$  is the inverse of the temperature and  $x_{i,d+1} = x_{i,1}, x_{d+1,j} = x_{1,j}$  for any  $1 \leq i, j \leq d$ .



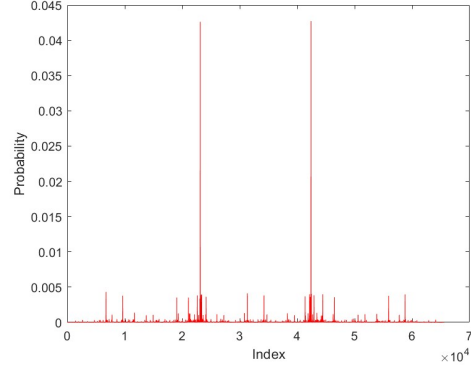
(a) Box plot with fixed sample size



(b) Error plot with varying sample sizes



(c) Target Distribution



(d) Generated Empirical Distribution

Figure 13: Two-dimensional antiferromagnetic Ising model with  $\beta = 0.3$  and  $d = 4$ ; (a) Box plot with fixed sample size  $N = 512$ ; (b) Error plot with varying sample sizes  $N \in \{64, 128, 256, 512, 1024\}$ ; (c) Target distribution; (d) Empirical distribution formed by samples generated by Algorithm 3.2 (sample size  $N = 65536$ ).

For our experiments on the two-dimensional Ising models, we pick  $\beta = 0.3, d = 4$  and the number of time steps to be  $L = 64$ . The initial distribution is selected to be the uniform distribution over  $\{-1, 1\}^{16}$ . Again, we fix the sample size to be  $N = 512$  for the experiments producing box plots. For the experiments studying how the loss function  $\mathcal{L}_2(\hat{p}, p)$  scales with respect to the sample size, we set the range of the sample sizes to be  $N \in \{64, 128, 256, 512, 1024\}$ . Finally, we set the sample size to be  $N = 65536$  in our visualization of the empirical distribution formed by the samples generated by Algorithm 3.2.

Similar to subsection 4.2.1 above, we test the three algorithms on both the ferromagnetic

and antiferromagnetic two-dimensional Ising models, whose interaction coefficients in (4.11) are given by  $J = -1$  and  $J = 1$  respectively. For the ferromagnetic model, whose testing results are listed in Figure (12), we again observe that the ensemble-based AIS performs better than the other two algorithms. Regarding the antiferromagnetic model, a comparison between the sub-figures given in Figure (13) leads to the same conclusion.

**5. Conclusion and Discussion.** In this paper, we considered the task of sampling multimodal distributions and proposed an improved version of AIS by combining it with ensemble-based Monte Carlo methods. Our method leverages the interaction between different particles in the ensemble, which allows us to find undiscovered modes more effectively. Regarding future work, one potential direction is to investigate how the ensemble-based methods can be combined with other continuation methods like Simulated Tempering and Tempered Transitions. Another interesting project is to study how the ensemble-based AIS may be used to sample distributions with approximate symmetries under the framework proposed in [102]. Moreover, studying the theoretical properties of the mean-field PDE derived (3.3) under appropriate assumptions on the acceptance ratio function  $A_t$  may also be of interest.

**Acknowledgments.** Haoxuan Chen would like to thank Dr. Yifan Chen for many helpful discussions on sampling-related problems and Xun Tang for proofreading an early draft of this manuscript.

**Appendix A: Derivation of the Weight in AIS Under the Continuum Limit.** Using integration by parts along with the given assumption that  $c(0) = 0$  and  $c(1) = 1$ , we have that

$$\begin{aligned}
 w &= U_0(x(0)) - U(x(1)) + \int_0^1 \langle \dot{x}, \nabla_x U_t(x) \rangle dt \\
 &= U_0(x(0)) - U(x(1)) + \int_0^1 (1 - c(t)) \langle \dot{x}, \nabla U_0(x) \rangle dt + \int_0^1 c(t) \langle \dot{x}, \nabla U(x) \rangle dt \\
 &= U_0(x(0)) - U(x(1)) + \int_0^1 (1 - c(t)) \cdot \frac{d}{dt} U_0(x(t)) dt + \int_0^1 c(t) \cdot \frac{d}{dt} U(x(t)) dt \\
 &= U_0(x(0)) - U(x(1)) + \int_0^1 c'(t) U_0(x(t)) dt + (1 - c(1)) U_0(x(1)) - (1 - c(0)) U_0(x(0)) \\
 &\quad - \int_0^1 c'(t) U(x(t)) dt + c(1) U(x(1)) - c(0) U(x(0)) \\
 &= - \int_0^1 c'(t) (U(x(t)) - U_0(x(t))) dt = - \int_0^1 \frac{\partial}{\partial t} U_t(x) dt.
 \end{aligned}$$

#### Appendix B: Derivation of the PDE (3.3).

*Proof.* We note that the main derivation of the proof utilizes the theory of measure-valued Markov processes [14], which is similar to that of [59, 83]. We begin by introducing a few notations used in the proof. For any smooth functional  $\Psi \in \mathcal{B}(\mathcal{P}(\mathbb{R}^d), \mathbb{R})$  and any measure  $\mu \in \mathcal{P}(\mathbb{R}^d)$ , the functional derivative of  $\Psi$  evaluated at  $\mu$  is defined to be a function  $D_\mu \Psi : \mathbb{R}^d \rightarrow \mathbb{R}$  such that the following identity holds for any signed measure  $\nu$  satisfying

$$\int_{\mathbb{R}^d} \nu(x) dx = 0:$$

$$(5.1) \quad \lim_{\epsilon \rightarrow 0} \frac{\Psi(\mu + \epsilon \nu) - \Psi(\mu)}{\epsilon} = \int_{\mathbb{R}^d} D_\mu \Psi(x) \nu(x) dx.$$

Moreover, for any time  $t \in [0, 1]$ , empirical measure  $\mu_N \in \mathcal{P}_N(\mathbb{R}^d)$  and smooth functional  $\Psi \in \mathcal{B}(\mathcal{P}(\mathbb{R}^d), \mathbb{R})$ , we define the time-dependent infinitesimal generator  $\mathcal{L}_{N,t}$  associated with the measure-valued markov process  $\mu_N^{(t)}$  as below:

$$(5.2) \quad (\mathcal{L}_{N,t} \Psi)(\mu_N) := \lim_{\Delta t \rightarrow 0^+} \frac{\mathbb{E}[\Psi(\mu_N^{(t+\Delta t)}) \mid \mu_N^{(t)} = \mu_N] - \Psi(\mu_N)}{\Delta t}.$$

To evaluate the infinitesimal generator defined above, we need to explicitly depict the change of the empirical measure caused by the stretch move and the birth-death dynamics. On the one hand, after a stretch move going from  $(x, y)$  to  $(z, y)$  happens at time  $t$ , we define the changed empirical measure to be

$$(5.3) \quad \mu_{N,S}^{(t)}\{(x, y) \rightarrow (z, y)\} := \mu_N^{(t)} + \frac{1}{N}(\delta_z - \delta_x).$$

On the other hand, after a swap between two particles  $x$  and  $x'$  happens at time  $t$  under the birth-death dynamics, we denote the changed empirical measure by

$$(5.4) \quad \mu_{N,BD}^{(t)}\{x \leftrightarrow x'\} := \mu_N^{(t)} - \frac{1}{N} \text{sign}(\beta^{(t)}(x, \mu_N^{(t)}))(\delta_x - \delta_{x'}),$$

where the birth-death rate function  $\beta^{(t)}(\cdot, \cdot) : \mathbb{R}^d \times \mathcal{P}(\mathbb{R}^d) \rightarrow \mathbb{R}$  above is defined as

$$(5.5) \quad \begin{aligned} \beta^{(t)}(x, \mu) &:= \frac{\partial}{\partial t} U_t(x) - \int_{\mathbb{R}^d} \frac{\partial}{\partial t} U_t(y) \mu(y) dy \\ &= c'(t) \left( U(x) - U_0(x) \right) - \int_{\mathbb{R}^d} c'(t) \left( U(y) - U_0(y) \right) \mu(y) dy. \end{aligned}$$

Recall that each particle  $x_i^{(t)}$  is also driven by the Langevin dynamics before the stretch move and the birth-death dynamics. Combining such fact with (5.3) and (5.4) defined above allows us to express the generator  $\mathcal{L}_{N,t}$  defined in (5.2) above as

$$(5.6) \quad \begin{aligned} (\mathcal{L}_{N,t} \Psi)(\mu_N) &= \frac{1}{N} \sum_{i=1}^N \int_{\mathbb{R}^d} \left( - \langle \nabla_x D_{\mu_N} \Psi(x), \nabla_x U_t(x) \rangle + \Delta_x D_{\mu_N} \Psi(x) \right) \delta_{x_i^{(t)}}(x) dx \\ &+ \sum_{i=1}^N \int_{\mathbb{R}^d} \left( \frac{1}{N} \sum_{j=1}^N \int_{\mathbb{R}^d} \left( \int_{\frac{1}{a}}^a \left( \Psi(\mu_{N,S}^{(t)}\{(x, y) \rightarrow (\lambda x + (1-\lambda)y, y)\}) - \Psi(\mu_N^{(t)}) \right) \right. \right. \\ &\cdot g(\lambda) A_t(x, y, \lambda) d\lambda \Big) \delta_{x_j^{(t)}}(y) dy \Big) \delta_{x_i^{(t)}}(x) dx \\ &+ \sum_{i=1}^N \int_{\mathbb{R}^d} \left( \frac{1}{N} \sum_{j=1}^N \int_{\mathbb{R}^d} \left( \Psi(\mu_{N,BD}^{(t)}\{x \leftrightarrow x'\}) - \Psi(\mu_N^{(t)}) \right) \right. \\ &\cdot \delta_{x_j^{(t)}}(x') dx' \Big) |\beta^{(t)}(x, \mu_N^{(t)})| \delta_{x_i^{(t)}}(x) dx, \end{aligned}$$

where  $\mu_N = \mu_N^{(t)} = \frac{1}{N} \sum_{i=1}^N x_i^{(t)}$ . Using the definition of functional derivatives in (5.1) along with the definition of changed measures in (5.3) and (5.4), one may further simplify the second term in (5.6), which corresponds to the stretch move, as follows:

$$\begin{aligned}
 (5.7) \quad & \sum_{i=1}^N \int_{\mathbb{R}^d} \left( \frac{1}{N} \sum_{j=1}^N \int_{\mathbb{R}^d} \left( \int_{\frac{1}{a}}^a \left( \frac{1}{N} \int_{\mathbb{R}^d} (D_{\mu_N} \Psi)(z) (\delta_{\lambda x + (1-\lambda)y}(z) - \delta_x(z)) dz \right) \right. \right. \\
 & \cdot g(\lambda) A_t(x, y, \lambda) d\lambda \Big) \delta_{x_j^{(t)}}(y) dy \Big) \delta_{x_i^{(t)}}(x) dx \\
 & = \int_{\mathbb{R}^d} \left( \int_{\mathbb{R}^d} \int_{\frac{1}{a}}^a (D_{\mu_N} \Psi)(\lambda x + (1-\lambda)y) g(\lambda) A_t(x, y, \lambda) \mu_N(y) d\lambda dy \right) \mu_N(x) dx \\
 & - \int_{\mathbb{R}^d} \left( \int_{\mathbb{R}^d} \int_{\frac{1}{a}}^a (D_{\mu_N} \Psi)(x) g(\lambda) A_t(x, y, \lambda) \mu_N(y) d\lambda dy \right) \mu_N(x) dx.
 \end{aligned}$$

Similarly, the third term in (5.6), which corresponds to the birth-death dynamics, can be further rewritten as

$$\begin{aligned}
 (5.8) \quad & \sum_{i=1}^N \int_{\mathbb{R}^d} \left( \frac{1}{N} \sum_{j=1}^N \int_{\mathbb{R}^d} \left( -\frac{1}{N} \int_{\mathbb{R}^d} (D_{\mu_N} \Psi)(z) \cdot \text{sign}(\beta^{(t)}(x, \mu_N)) (\delta_x(z) - \delta_{x'}(z)) dz \right) \right. \\
 & \cdot \delta_{x_j^{(t)}}(x') dx' \Big) |\beta^{(t)}(x, \mu_N)| \delta_{x_i^{(t)}}(x) dx \\
 & = - \int_{\mathbb{R}^d} (D_{\mu_N} \Psi)(x) \beta^{(t)}(x, \mu_N) \mu_N(x) dx + \left( \int_{\mathbb{R}^d} (D_{\mu_N} \Psi)(x') \mu_N(x') dx' \right) \\
 & \cdot \left( \int_{\mathbb{R}^d} \beta^{(t)}(x, \mu_N) \mu_N(x) dx \right).
 \end{aligned}$$

Plugging in (5.7) and (5.8) then gives us a simplified form of the generator  $\mathcal{L}_{N,t}$ :

$$\begin{aligned}
 (5.9) \quad & (\mathcal{L}_{N,t} \Psi)(\mu_N) = \int_{\mathbb{R}^d} \left( -\langle \nabla_x (D_{\mu_N} \Psi)(x), \nabla_x U_t(x) \rangle + \Delta_x (D_{\mu_N} \Psi)(x) \right) \mu_N(x) dx \\
 & + \int_{\mathbb{R}^d} \left( \int_{\mathbb{R}^d} \int_{\frac{1}{a}}^a (D_{\mu_N} \Psi)(\lambda x + (1-\lambda)y) g(\lambda) A_t(x, y, \lambda) \mu_N(y) d\lambda dy \right) \mu_N(x) dx \\
 & - \int_{\mathbb{R}^d} \left( \int_{\mathbb{R}^d} \int_{\frac{1}{a}}^a (D_{\mu_N} \Psi)(x) g(\lambda) A_t(x, y, \lambda) \mu_N(y) d\lambda dy \right) \mu_N(x) dx \\
 & - \int_{\mathbb{R}^d} (D_{\mu_N} \Psi)(x) \beta^{(t)}(x, \mu_N) \mu_N(x) dx + \left( \int_{\mathbb{R}^d} (D_{\mu_N} \Psi)(x') \mu_N(x') dx' \right) \\
 & \cdot \left( \int_{\mathbb{R}^d} \beta^{(t)}(x, \mu_N) \mu_N(x) dx \right).
 \end{aligned}$$

Using the generator  $\mathcal{L}_{N,t}$  derived above, we may write out the backward Kolmogorov equation of  $\Psi(\mu_N^{(t)})$  as follows:

$$(5.10) \quad \frac{\partial}{\partial t} \Psi(\mu_N^{(t)}) = (\mathcal{L}_{N,t} \Psi)(\mu_N^{(t)}), \quad \Psi(\mu_N^{(t)})|_{t=0} = \Psi(\mu_N^{(0)}).$$

Now, we may consider the equation above under the mean-field limit  $N \rightarrow \infty$ . Given that  $\mu_N^{(0)}$  converges to some  $\rho_0$  in law as  $N \rightarrow \infty$ , we have that  $\mu_N^{(t)}$  converges in law to some  $\rho_t(\cdot) = \rho(t, \cdot)$  as  $N \rightarrow \infty$  for any  $t \in [0, 1]$ , where  $\Psi(\rho_t)$  solves the following mean-field backward Kolmogorov equation for any fixed  $\Psi \in \mathcal{B}(\mathcal{P}(\mathbb{R}^d), \mathbb{R})$ :

$$(5.11) \quad \frac{\partial}{\partial t} \Psi(\rho_t) = (\mathcal{L}_t \Psi)(\rho_t), \quad \Psi(\rho_t)|_{t=0} = \Psi(\rho_0).$$

Above the limiting operator  $\mathcal{L}_t = \lim_{N \rightarrow \infty} \mathcal{L}_{N,t}$  is obtained by replacing the empirical measure  $\mu_N$  with a generic measure  $\rho$ , i.e.,

$$(5.12) \quad \begin{aligned} (\mathcal{L}_t \Psi)(\rho) &= \int_{\mathbb{R}^d} \left( -\langle \nabla_x (D_\rho \Psi)(x), \nabla_x U_t(x) \rangle + \Delta_x (D_\rho \Psi)(x) \right) \rho(x) dx \\ &+ \int_{\mathbb{R}^d} \left( \int_{\mathbb{R}^d} \int_{\frac{1}{a}}^a (D_\rho \Psi)(\lambda x + (1-\lambda)y) g(\lambda) A_t(x, y, \lambda) \rho(y) d\lambda dy \right) \rho(x) dx \\ &- \int_{\mathbb{R}^d} \left( \int_{\mathbb{R}^d} \int_{\frac{1}{a}}^a (D_\rho \Psi)(x) g(\lambda) A_t(x, y, \lambda) \rho(y) d\lambda dy \right) \rho(x) dx \\ &- \int_{\mathbb{R}^d} (D_\rho \Psi)(x) \beta^{(t)}(x, \rho) \rho(x) dx + \left( \int_{\mathbb{R}^d} (D_\rho \Psi)(x') \rho(x') dx' \right) \\ &\cdot \left( \int_{\mathbb{R}^d} \beta^{(t)}(x, \rho) \rho(x) dx \right), \end{aligned}$$

for any  $\Psi \in \mathcal{B}(\mathcal{P}(\mathbb{R}^d), \mathbb{R})$  and  $\rho \in \mathcal{P}(\mathbb{R}^d)$ . Now it suffices to show that  $\Psi(\rho_t)$  evolves according to equation (5.11) when  $\rho_t$  solves the PDE (3.3), which requires us to simplify further the expression given in (5.12). Firstly, we may apply integration by parts to rewrite the first term in (5.12) as below:

$$(5.13) \quad \begin{aligned} &\int_{\mathbb{R}^d} \left( -\langle \nabla_x D_\rho \Psi(x), \nabla_x U_t(x) \rangle + \Delta_x (D_\rho \Psi)(x) \right) \rho(x) dx \\ &= \int_{\mathbb{R}^d} (D_\rho \Psi)(x) \left( \nabla_x \cdot (\nabla_x U_t(x) \rho(x)) + \Delta_x \rho(x) \right) dx. \end{aligned}$$

Secondly, we consider using a change of variables to rewrite the second term in (5.12). Note that for fixed  $y \in \mathbb{R}^d$ , the Jacobian of the transform  $(x, \lambda) \rightarrow (z, \alpha)$  defined via  $z = \lambda x + (1-\lambda)y$  and  $\alpha = \lambda^{-1}$  satisfies  $\left| \det \left( \frac{\partial(x, \lambda)}{\partial(z, \alpha)} \right) \right| = |\alpha^d| |\alpha^{-2}| = |\alpha|^{d-2}$ . Then we may use  $(z, \lambda)$  to rewrite

the second term in (5.12) in the following way:

$$\begin{aligned}
 & \int_{\mathbb{R}^d} \left( \int_{\mathbb{R}^d} \int_{\frac{1}{a}}^a (D_\rho \Psi)(\lambda x + (1-\lambda)y) g(\lambda) A_t(x, y, \lambda) \rho(x) d\lambda dx \right) \rho(y) dy \\
 &= \int_{\mathbb{R}^d} \left( \int_{\mathbb{R}^d} \int_{\frac{1}{a}}^a (D_\rho \Psi)(z) g(\alpha^{-1}) A_t(\alpha z + (1-\alpha)y, y, \alpha^{-1}) \right. \\
 (5.14) \quad & \cdot \rho(\alpha z + (1-\alpha)y) |\alpha|^{d-2} d\alpha dz \Big) \rho(y) dy \\
 &= \int_{\mathbb{R}^d} (D_\rho \Psi)(z) \left( \int_{\frac{1}{a}}^a |\alpha|^{d-2} g(\alpha^{-1}) \left( \int_{\mathbb{R}^d} A_t(\alpha z + (1-\alpha)y, y, \alpha^{-1}) \right. \right. \\
 & \cdot \rho(y) \rho(\alpha z + (1-\alpha)y) dy \Big) d\alpha \Big) dz
 \end{aligned}$$

Thirdly, plugging in the expression of the rate function given in (5.5) allows us to rewrite the fourth and fifth terms in (5.12) as follows:

$$\begin{aligned}
 & - \int_{\mathbb{R}^d} (D_\rho \Psi)(x) \beta^{(t)}(x, \rho) \rho(x) dx + \left( \int_{\mathbb{R}^d} (D_\rho \Psi)(x') \rho(x') dx' \right) \\
 (5.15) \quad & \cdot \left( \int_{\mathbb{R}^d} \left( \frac{\partial}{\partial t} U_t(x) - \int_{\mathbb{R}^d} \frac{\partial}{\partial t} U_t(y) \rho(y) dy \right) \rho(x) dx \right) \\
 &= - \int_{\mathbb{R}^d} (D_\rho \Psi)(x) \beta^{(t)}(x, \rho) \rho(x) dx \\
 &= - \int_{\mathbb{R}^d} (D_\rho \Psi)(x) \left( \frac{\partial}{\partial t} U_t(x) - \int_{\mathbb{R}^d} \frac{\partial}{\partial t} U_t(y) \rho(y) dy \right) \rho(x) dx
 \end{aligned}$$

Finally, by substituting (5.13), (5.14) and (5.15) and switching the variables in (5.14), we obtain that

$$\begin{aligned}
 (\mathcal{L}_t \Psi)(\rho) &= \int_{\mathbb{R}^d} (D_\rho \Psi)(x) \left( \left( \nabla_x \cdot (\nabla_x U_t(x) \rho(x)) + \Delta_x \rho(x) \right) \right. \\
 (5.16) \quad & + \int_{\frac{1}{a}}^a |\lambda|^{d-2} g(\lambda^{-1}) \left( \int_{\mathbb{R}^d} A_t(\lambda x + (1-\lambda)y, y, \lambda^{-1}) \rho(y) \rho(\lambda x + (1-\lambda)y) dy \right) d\lambda \\
 & - \left( \int_{\frac{1}{a}}^a g(\lambda) \left( \int_{\mathbb{R}^d} A_t(x, y, \lambda) \rho(y) dy \right) d\lambda \right) \rho(x) \\
 & \left. - \left( \frac{\partial}{\partial t} U_t(x) - \int_{\mathbb{R}^d} \frac{\partial}{\partial t} U_t(y) \rho(y) dy \right) \rho(x) \right) dx.
 \end{aligned}$$

Comparing (5.16) with the RHS of (3.3) and plugging in  $U_t(x) = (1-c(t))U_0(x) + c(t)U(x)$  indicate that the PDE governing the evolution of  $\Psi(\rho_t)$  is indeed (5.11) when  $\rho_t$  solves (3.3), as desired.

## REFERENCES



- [1] M. S. ALBERGO, N. M. BOFFI, AND E. VANDEN-EIJNDEN, *Stochastic interpolants: A unifying framework for flows and diffusions*, arXiv preprint arXiv:2303.08797, (2023).
- [2] H. C. ANDERSEN, *Molecular dynamics simulations at constant pressure and/or temperature*, The Journal of chemical physics, 72 (1980), pp. 2384–2393.
- [3] I. ANDRICIOAEI, J. E. STRAUB, AND A. F. VOTER, *Smart darting monte carlo*, The Journal of Chemical Physics, 114 (2001), pp. 6994–7000.
- [4] J. BIERKENS, P. FEARNHEAD, AND G. ROBERTS, *The zig-zag process and super-efficient sampling for bayesian analysis of big data*, (2019).
- [5] A. BOUCHARD-CÔTÉ, S. J. VOLLMER, AND A. DOUCET, *The bouncy particle sampler: A nonreversible rejection-free markov chain monte carlo method*, Journal of the American Statistical Association, 113 (2018), pp. 855–867.
- [6] C. J. T. BRAAK, *A markov chain monte carlo version of the genetic algorithm differential evolution: easy bayesian computing for real parameter spaces*, Statistics and Computing, 16 (2006), pp. 239–249.
- [7] Y. CAO AND E. VANDEN-EIJNDEN, *Learning optimal flows for non-equilibrium importance sampling*, Advances in Neural Information Processing Systems, 35 (2022), pp. 12352–12364.
- [8] D. CARBONE, M. HUA, S. COSTE, AND E. VANDEN-EIJNDEN, *Efficient training of energy-based models using jarzynski equality*, arXiv preprint arXiv:2305.19414, (2023).
- [9] J. A. CARRILLO, F. HOFFMANN, A. M. STUART, AND U. VAES, *Consensus-based sampling*, Studies in Applied Mathematics, 148 (2022), pp. 1069–1140.
- [10] Y. CHEN, D. Z. HUANG, J. HUANG, S. REICH, AND A. M. STUART, *Sampling via gradient flows in the space of probability measures*, arXiv preprint arXiv:2310.03597, (2023).
- [11] X. CHENG, N. S. CHATTERJI, P. L. BARTLETT, AND M. I. JORDAN, *Underdamped langevin mcmc: A non-asymptotic analysis*, in Conference on learning theory, PMLR, 2018, pp. 300–323.
- [12] J. COULLON AND R. J. WEBBER, *Ensemble sampler for infinite-dimensional inverse problems*, Statistics and Computing, 31 (2021), pp. 1–9.
- [13] A. S. DALALYAN, *Theoretical guarantees for approximate sampling from smooth and log-concave densities*, Journal of the Royal Statistical Society Series B: Statistical Methodology, 79 (2017), pp. 651–676.
- [14] D. A. DAWSON, B. MAISONNEUVE, J. SPENCER, AND D. DAWSON, *Measure-valued Markov processes*, Springer, 1993.
- [15] P. DEL MORAL, A. DOUCET, AND A. JASRA, *Sequential monte carlo samplers*, Journal of the Royal Statistical Society Series B: Statistical Methodology, 68 (2006), pp. 411–436.
- [16] X. DING AND D. J. FREEDMAN, *Learning deep generative models with annealed importance sampling*, arXiv preprint arXiv:1906.04904, (2019).
- [17] Z. DING AND Q. LI, *Ensemble kalman sampler: Mean-field limit and convergence analysis*, SIAM Journal on Mathematical Analysis, 53 (2021), pp. 1546–1578.
- [18] A. R. DINNER, E. H. THIEDE, B. V. KOTEN, AND J. WEARE, *Stratification as a general variance reduction method for markov chain monte carlo*, SIAM/ASA journal on uncertainty quantification, 8 (2020), pp. 1139–1188.
- [19] A. DOUCET, W. GRATHWOHL, A. G. MATTHEWS, AND H. STRATHMANN, *Score-based diffusion meets annealed importance sampling*, Advances in Neural Information Processing Systems, 35 (2022), pp. 21482–21494.
- [20] A. DOUCET, A. M. JOHANSEN, ET AL., *A tutorial on particle filtering and smoothing: Fifteen years later*, Handbook of nonlinear filtering, 12 (2009), p. 3.
- [21] S. DUANE, A. D. KENNEDY, B. J. PENDLETON, AND D. ROWETH, *Hybrid monte carlo*, Physics letters B, 195 (1987), pp. 216–222.
- [22] M. M. DUNLOP AND G. STADLER, *A gradient-free subspace-adjusting ensemble sampler for infinite-dimensional bayesian inverse problems*, arXiv preprint arXiv:2202.11088, (2022).
- [23] A. DURMUS AND E. MOULINES, *Nonasymptotic convergence analysis for the unadjusted langevin algorithm*, The annals of applied probability, 27 (2017), pp. 1551–1587.
- [24] R. DWIVEDI, Y. CHEN, M. J. WAINWRIGHT, AND B. YU, *Log-concave sampling: Metropolis-hastings algorithms are fast!*, in Conference on learning theory, PMLR, 2018, pp. 793–797.
- [25] W. E, W. REN, AND E. VANDEN-EIJNDEN, *Minimum action method for the study of rare events*, Communications on pure and applied mathematics, 57 (2004), pp. 637–656.

- [26] M. GABRIÉ, G. M. ROTSKOFF, AND E. VANDEN-EIJNDEN, *Adaptive monte carlo augmented with normalizing flows*, Proceedings of the National Academy of Sciences, 119 (2022), p. e2109420119.
- [27] A. GARBUNO-INIGO, F. HOFFMANN, W. LI, AND A. M. STUART, *Interacting langevin diffusions: Gradient structure and ensemble kalman sampler*, SIAM Journal on Applied Dynamical Systems, 19 (2020), pp. 412–441.
- [28] A. GARBUNO-INIGO, N. NÜSKEN, AND S. REICH, *Affine invariant interacting langevin dynamics for bayesian inference*, SIAM Journal on Applied Dynamical Systems, 19 (2020), pp. 1633–1658.
- [29] A. GELMAN, W. R. GILKS, AND G. O. ROBERTS, *Weak convergence and optimal scaling of random walk metropolis algorithms*, The annals of applied probability, 7 (1997), pp. 110–120.
- [30] C. J. GEYER, *Markov chain monte carlo maximum likelihood*, in E. M. Kernamidas, editor, Computing Science and Statistics: Proc. 23rd Symposium on the Interface, Interface Foundation of North America, 1991, pp. 156–163.
- [31] C. J. GEYER AND E. A. THOMPSON, *Annealing markov chain monte carlo with applications to ancestral inference*, Journal of the American Statistical Association, 90 (1995), pp. 909–920.
- [32] W. R. GILKS, G. O. ROBERTS, AND E. I. GEORGE, *Adaptive direction sampling*, Journal of the Royal Statistical Society: Series D (The Statistician), 43 (1994), pp. 179–189.
- [33] R. J. GLAUBER, *Time-dependent statistics of the ising model*, Journal of mathematical physics, 4 (1963), pp. 294–307.
- [34] J. GOODMAN AND J. WEARE, *Ensemble samplers with affine invariance*, Communications in applied mathematics and computational science, 5 (2010), pp. 65–80.
- [35] K.-H. HOFFMANN AND Q. TANG, *Ginzburg-Landau phase transition theory and superconductivity*, vol. 134, Birkhäuser, 2012.
- [36] P. C. HOHENBERG AND A. P. KREKHOV, *An introduction to the ginzburg-landau theory of phase transitions and nonequilibrium patterns*, Physics Reports, 572 (2015), pp. 1–42.
- [37] J. H. HOLLAND, *Adaptation in natural and artificial systems: an introductory analysis with applications to biology, control, and artificial intelligence*, MIT press, 1992.
- [38] K. HUKUSHIMA AND K. NEMOTO, *Exchange monte carlo method and application to spin glass simulations*, Journal of the Physical Society of Japan, 65 (1996), pp. 1604–1608.
- [39] A. I. N. IBRAHIM, *New methods for mode jumping in Markov chain Monte Carlo algorithms*, PhD thesis, University of Bath, 2009.
- [40] C. JARZYNSKI, *Nonequilibrium equality for free energy differences*, Physical Review Letters, 78 (1997), p. 2690.
- [41] M. KARAMANIS AND F. BEUTLER, *Ensemble slice sampling: Parallel, black-box and gradient-free inference for correlated & multimodal distributions*, Statistics and Computing, 31 (2021), pp. 1–18.
- [42] S. KOU, Q. ZHOU, AND W. H. WONG, *Equi-energy sampler with applications in statistical inference and statistical mechanics*, The Annals of Statistics, 34 (2006), pp. 1581–1619.
- [43] B. LEIMKUHLER, C. MATTHEWS, AND J. WEARE, *Ensemble preconditioning for markov chain monte carlo simulation*, Statistics and Computing, 28 (2018), pp. 277–290.
- [44] F. LIANG, *Use of sequential structure in simulation from high-dimensional systems*, Physical Review E, 67 (2003), p. 056101.
- [45] F. LIANG, C. LIU, AND R. CARROLL, *Advanced Markov chain Monte Carlo methods: learning from past samples*, vol. 714, John Wiley & Sons, 2011.
- [46] F. LIANG AND W. H. WONG, *Evolutionary monte carlo for protein folding simulations*, The Journal of Chemical Physics, 115 (2001), pp. 3374–3380.
- [47] F. LIANG AND W. H. WONG, *Real-parameter evolutionary monte carlo with applications to bayesian mixture models*, Journal of the American Statistical Association, 96 (2001), pp. 653–666.
- [48] E. M. LIFSHITZ AND L. P. PITAEVSKII, *Statistical physics: theory of the condensed state*, vol. 9, Elsevier, 2013.
- [49] M. LINDSEY, J. WEARE, AND A. ZHANG, *Ensemble markov chain monte carlo with teleporting walkers*, SIAM/ASA Journal on Uncertainty Quantification, 10 (2022), pp. 860–885.
- [50] J. S. LIU, F. LIANG, AND W. H. WONG, *The multiple-try method and local optimization in metropolis sampling*, Journal of the American Statistical Association, 95 (2000), pp. 121–134.
- [51] J. S. LIU AND J. S. LIU, *Monte Carlo strategies in scientific computing*, vol. 75, Springer, 2001.
- [52] J. S. LIU AND C. SABATTI, *Generalised gibbs sampler and multigrid monte carlo for bayesian computa-*

- tion, *Biometrika*, 87 (2000), pp. 353–369.
- [53] Q. LIU, *Stein variational gradient descent as gradient flow*, *Advances in neural information processing systems*, 30 (2017).
  - [54] Q. LIU AND D. WANG, *Stein variational gradient descent: A general purpose bayesian inference algorithm*, *Advances in neural information processing systems*, 29 (2016).
  - [55] Z. LIU, A. M. STUART, AND Y. WANG, *Second order ensemble langevin method for sampling and inverse problems*, arXiv preprint arXiv:2208.04506, (2022).
  - [56] S. LIVINGSTONE, M. BETANCOURT, S. BYRNE, AND M. GIROLAMI, *On the geometric ergodicity of hamiltonian monte carlo*, (2019).
  - [57] J. LU, Y. LU, AND J. NOLEN, *Scaling limit of the stein variational gradient descent: The mean field regime*, *SIAM Journal on Mathematical Analysis*, 51 (2019), pp. 648–671.
  - [58] J. LU AND L. WANG, *Complexity of zigzag sampling algorithm for strongly log-concave distributions*, *Statistics and Computing*, 32 (2022), p. 48.
  - [59] Y. LU, J. LU, AND J. NOLEN, *Accelerating langevin sampling with birth-death*, arXiv preprint arXiv:1905.09863, (2019).
  - [60] Y. LU, D. SLEPČEV, AND L. WANG, *Birth–death dynamics for sampling: global convergence, approximations and their asymptotics*, *Nonlinearity*, 36 (2023), p. 5731.
  - [61] E. LYMAN AND D. M. ZUCKERMAN, *Annealed importance sampling of peptides*, *The Journal of chemical physics*, 127 (2007).
  - [62] S. N. MACÉACHERN, M. CLYDE, AND J. S. LIU, *Sequential importance sampling for nonparametric bayes models: The next generation*, *Canadian Journal of Statistics*, 27 (1999), pp. 251–267.
  - [63] O. MANGOUBI AND A. SMITH, *Rapid mixing of hamiltonian monte carlo on strongly log-concave distributions*, arXiv preprint arXiv:1708.07114, (2017).
  - [64] E. MARINARI AND G. PARISI, *Simulated tempering: a new monte carlo scheme*, *Europhysics letters*, 19 (1992), p. 451.
  - [65] Y. MARZOUK, T. MOSELHY, M. PARNO, AND A. SPANTINI, *Sampling via measure transport: An introduction*, *Handbook of uncertainty quantification*, 1 (2016), p. 2.
  - [66] C. MATTHEWS, J. WEARE, A. KRAVTSOV, AND E. JENNINGS, *Umbrella sampling: A powerful method to sample tails of distributions*, *Monthly Notices of the Royal Astronomical Society*, 480 (2018), pp. 4069–4079.
  - [67] A. MAURAS AND Y. MARZOUK, *Sampling in unit time with kernel fisher-rao flow*, arXiv preprint arXiv:2401.03892, (2024).
  - [68] L. I. MIDGLEY, V. STIMPER, G. N. SIMM, B. SCHÖLKOPF, AND J. M. HERNÁNDEZ-LOBATO, *Flow annealed importance sampling bootstrap*, arXiv preprint arXiv:2208.01893, (2022).
  - [69] R. M. NEAL, *Sampling from multimodal distributions using tempered transitions*, *Statistics and computing*, 6 (1996), pp. 353–366.
  - [70] R. M. NEAL, *Annealed importance sampling*, *Statistics and computing*, 11 (2001), pp. 125–139.
  - [71] R. M. NEAL ET AL., *Mcmc using hamiltonian dynamics*, *Handbook of markov chain monte carlo*, 2 (2011), p. 2.
  - [72] R. M. NEAL AND R. M. NEAL, *Monte carlo implementation*, *Bayesian learning for neural networks*, (1996), pp. 55–98.
  - [73] M. D. PARNO AND Y. M. MARZOUK, *Transport map accelerated markov chain monte carlo*, *SIAM/ASA Journal on Uncertainty Quantification*, 6 (2018), pp. 645–682.
  - [74] Y. PENG, Y. CHEN, E. M. SToudenMIRE, AND Y. KHOO, *Generative modeling via hierarchical tensor sketching*, arXiv preprint arXiv:2304.05305, (2023).
  - [75] J. PIDSTRIGACH AND S. REICH, *Affine-invariant ensemble transform methods for logistic regression*, *Foundations of Computational Mathematics*, 23 (2023), pp. 675–708.
  - [76] E. POMPE, C. HOLMES, AND K. LATUSZYŃSKI, *A framework for adaptive mcmc targeting multimodal distributions*, *The Annals of Statistics*, 48 (2020), pp. 2930–2952.
  - [77] Y. REN, H. ZHAO, Y. KHOO, AND L. YING, *High-dimensional density estimation with tensorizing flow*, *Research in the Mathematical Sciences*, 10 (2023), p. 30.
  - [78] G. O. ROBERTS AND J. S. ROSENTHAL, *Optimal scaling of discrete approximations to langevin diffusions*, *Journal of the Royal Statistical Society: Series B (Statistical Methodology)*, 60 (1998), pp. 255–268.
  - [79] G. O. ROBERTS AND J. S. ROSENTHAL, *Optimal scaling for various metropolis-hastings algorithms*,

- Statistical science, 16 (2001), pp. 351–367.
- [80] G. O. ROBERTS AND O. STRAMER, *Langevin diffusions and metropolis-hastings algorithms*, Methodology and computing in applied probability, 4 (2002), pp. 337–357.
  - [81] G. O. ROBERTS AND R. L. TWEEDIE, *Exponential convergence of langevin distributions and their discrete approximations*, Bernoulli, (1996), pp. 341–363.
  - [82] P. J. ROSSKY, J. D. DOLL, AND H. L. FRIEDMAN, *Brownian dynamics as smart monte carlo simulation*, The Journal of Chemical Physics, 69 (1978), pp. 4628–4633.
  - [83] G. ROTSKOFF, S. JELASSI, J. BRUNA, AND E. VANDEN-EIJNDEN, *Neuron birth-death dynamics accelerates gradient descent and converges asymptotically*, in International Conference on Machine Learning, PMLR, 2019, pp. 5508–5517.
  - [84] C. SMINCHISCU AND M. WELLING, *Generalized darting monte carlo*, in Artificial Intelligence and Statistics, PMLR, 2007, pp. 516–523.
  - [85] C. SMINCHISCU, M. WELLING, AND G. HINTON, *A mode-hopping mcmc sampler*, tech. report, Technical Report CSRG-478, University of Toronto, submitted to Machine ... , 2003.
  - [86] B. SPRUNGK, S. WEISSMANN, AND J. ZECH, *Metropolis-adjusted interacting particle sampling*, arXiv preprint arXiv:2312.13889, (2023).
  - [87] A. S. STORDAL AND A. H. ELSHEIKH, *Iterative ensemble smoothers in the annealed importance sampling framework*, Advances in Water Resources, 86 (2015), pp. 231–239.
  - [88] R. H. SWENDSEN AND J.-S. WANG, *Nonuniversal critical dynamics in monte carlo simulations*, Physical review letters, 58 (1987), p. 86.
  - [89] L. TAN AND J. LU, *Accelerate langevin sampling with birth-death process and exploration component*, arXiv preprint arXiv:2305.05529, (2023).
  - [90] N. G. TAWN, M. T. MOORES, AND G. O. ROBERTS, *Annealed leap-point sampler for multimodal target distributions*, arXiv preprint arXiv:2112.12908, (2021).
  - [91] C. J. TER BRAAK AND J. A. VRUGT, *Differential evolution markov chain with snooker updater and fewer chains*, Statistics and Computing, 18 (2008), pp. 435–446.
  - [92] E. H. THIEDE, B. VAN KOTEN, J. WEARE, AND A. R. DINNER, *Eigenvector method for umbrella sampling enables error analysis*, The Journal of chemical physics, 145 (2016).
  - [93] H. TJELMELAND AND J. EIDSVIK, *On the use of local optimizations within metropolis–hastings updates*, Journal of the Royal Statistical Society Series B: Statistical Methodology, 66 (2004), pp. 411–427.
  - [94] H. TJELMELAND AND B. K. HEGSTAD, *Mode jumping proposals in mcmc*, Scandinavian journal of statistics, 28 (2001), pp. 205–223.
  - [95] F. VARGAS, W. GRATHWOHL, AND A. DOUCET, *Denoising diffusion samplers*, arXiv preprint arXiv:2302.13834, (2023).
  - [96] Y. WANG AND W. LI, *Accelerated information gradient flow*, Journal of Scientific Computing, 90 (2022), pp. 1–47.
  - [97] U. WOLFF, *Collective monte carlo updating for spin systems*, Physical Review Letters, 62 (1989), p. 361.
  - [98] K. WU, S. SCHMIDLER, AND Y. CHEN, *Minimax mixing time of the metropolis-adjusted langevin algorithm for log-concave sampling*, The Journal of Machine Learning Research, 23 (2022), pp. 12348–12410.
  - [99] M. YASUDA AND K. SEKIMOTO, *Spatial monte carlo integration with annealed importance sampling*, Physical Review E, 103 (2021), p. 052118.
  - [100] M. YASUDA AND C. TAKAHASHI, *Free energy evaluation using marginalized annealed importance sampling*, Physical Review E, 106 (2022), p. 024127.
  - [101] L. YING, *Annealed importance sampling for ising models with mixed boundary conditions*, Journal of Computational Mathematics, 41 (2023), pp. 542–550.
  - [102] L. YING, *Multimodal sampling via approximate symmetries*, arXiv preprint arXiv:2310.07244, (2023).
  - [103] G. ZHANG, K. HSU, J. LI, C. FINN, AND R. B. GROSSE, *Differentiable annealed importance sampling and the perils of gradient noise*, Advances in Neural Information Processing Systems, 34 (2021), pp. 19398–19410.